Journal of *Marine Science and Engineering*

MDPI

Article

The Potential of Wave Energy Conversion to Mitigate Coastal Erosion from Hurricanes

Cigdem Ozkan [1,*], Talea Mayo [2] and Davina L. Passeri [3]

[1] The Balmoral Group, Winter Park, FL 32789, USA
[2] Department of Mathematics, Emory University, Atlanta, GA 30322, USA; talea.mayo@emory.edu
[3] U.S. Geological Survey St. Petersburg Coastal and Marine Science Center, St. Petersburg, FL 33701, USA; dpasseri@usgs.gov
* Correspondence: COzkan@balmoralgroup.us

Abstract: Wave energy conversion technologies have recently attracted more attention as part of global efforts to replace fossil fuels with renewable energy resources. While ocean waves can provide renewable energy, they can also be destructive to coastal areas that are often densely populated and vulnerable to coastal erosion. There have been a variety of efforts to mitigate the impacts of wave- and storm-induced erosion; however, they are either temporary solutions or approaches that are not able to adapt to a changing climate. This study explores a green and sustainable approach to mitigating coastal erosion from hurricanes through wave energy conversion. A barrier island, Dauphin Island, off the coast of Alabama, is used as a test case. The potential use of wave energy converter farms to mitigate erosion due to hurricane storm surges while simultaneously generating renewable energy is explored through simulations that are forced with storm data using the XBeach model. It is shown that wave farms can impact coastal morphodynamics and have the potential to reduce dune and beach erosion, predominantly in the western portion of the island. The capacity of wave farms to influence coastal morphodynamics varies with the storm intensity.

Keywords: wave energy conversion; wave farm; coastal erosion; nearshore impact; XBeach

Citation: Ozkan, C.; Mayo, T.; Passeri, D.L. The Potential of Wave Energy Conversion to Mitigate Coastal Erosion from Hurricanes. *J. Mar. Sci. Eng.* **2022**, *10*, 143. https://doi.org/10.3390/jmse10020143

Academic Editor: Rafael Morales

Received: 13 December 2021
Accepted: 7 January 2022
Published: 21 January 2022

1. Introduction

Wave energy conversion is the process of converting the kinetic and potential energy of ocean waves into mechanical or electrical energy. Ocean wave energy is abundant, consistent, and is an emerging source of renewable energy [1]. Energy in the waves can be harnessed and converted into electricity through wave energy converter devices (WECs). WECs are commonly configured in arrays, i.e., wave farms, to increase the span across which waves can be captured, and optimize the use of materials such as underwater cables that are used to transfer the generated electricity to the shore. Although the initial cost of wave farms can be high [2,3], coastal communities can doubly benefit from them because they not only provide electricity but also have the potential to reduce coastal erosion.

Beach erosion is a global coastal hazard with catastrophic consequences due to the land and property loss that can ensue. Of the world's sandy beaches, 24% of them are experiencing erosion rates exceeding 0.5 m/yr [4]. In the United States, environmental agencies have described stretches of the Gulf of Mexico (GOM) and Atlantic coastlines as critically eroding [5]. The average coastal erosion rate along the Atlantic coast of the United States is reported to be 0.6 to 0.9 m/yr [6]. Coastal erosion rates are expected to increase in the coming years, and even those coastlines that are currently stable or accreting may begin to experience erosion [7]. Furthermore, coastal regions are often heavily urbanized and densely populated, comprising nearly 40% of the U.S. population [8]. The population in coastal areas increased by 39% from 1970 to 2010, and this upward trend is projected to continue [9]. The growing coastal population and climate change impacts (e.g., rising sea levels and increasing severity of tropical cyclones) make coastal regions increasingly

vulnerable to erosion [10]. An increase in coastal flood frequency and extreme events is expected over the coming decades, which will accelerate beach and cliff erosion [11].

As a result, efforts to mitigate the effects of coastal erosion have intensified. The construction of seawalls, breakwaters, revetments, and jetties, in addition to beach renourishment projects are some of the more traditional coastal engineering approaches to mitigation. However, these conventional methods may not adapt well to the changing climate, and nature-based solutions may offer a better alternative [12]. Greener options, including wetland protection and construction of living shorelines have been explored in recent years [13–15]. While these strategies provide solutions to coastal erosion, they fail to address the root causes of the hazard and often require substantial maintenance. For example, beach-nourishment projects in Sand Key, FL have been implemented 26 times since 1961, with a total cost of USD 142 million [16]. A seawall repair project in Ellis Island, NY proposed in 2010 is expected to cost stakeholders a total of USD 29 million in addition to the initial cost of construction [17].

In search of a sustainable approach to mitigating coastal erosion and utilizing marine energy resources, an increasing number of studies have begun to explore the impacts of WECs on coastal morphodynamics. While potentially harmful impacts of WECs to the environment (e.g., scour to the seabed, changes to water circulation and water quality, and attraction or repulsion of marine life) are continually being investigated [18,19], many studies have illustrated that they often mitigate coastal erosion for gravel and sandy beaches [20–22]. Specifically, wave dampening (i.e., removing the energy of the waves), wave reflection (i.e., acting as a physical barrier) [23–38], and reduction in the bottom shear stress [39,40] due to the presence of WECs can affect flow and energy in a way that can contribute to coastline vitality. Studies to date have been focused mostly in Europe, with one study in the United States carried out for Newport, OR [40]. In this study, we use the numerical morphological model XBeach to simulate the impacts of wave energy conversion on coastal erosion on a barrier island on the U.S Gulf Coast. We perform a case study, focused on Dauphin Island, AL, where we use XBeach to simulate baseline (i.e., with no wave farm) and wave farm scenarios under severe storm (Hurricane Ivan and Hurricane Katrina) conditions, and analyze the impact of WECs to beach profiles, dune heights, total water levels (TWL), i.e., total elevation of storm-induced water levels including storm surge, astronomical tide, and wave runup, bottom shear stresses, and total sediment volume/area of the coastline.

2. Case Study

2.1. Location

Dauphin Island is located in the northern Gulf of Mexico off the coast of mainland Alabama (Figure 1). It is a narrow, 25 km-long, low-lying barrier island with an average elevation of 2.18 m above mean sea level [41]. Dauphin Island has a diverse topography, with beaches, dunes, wetlands, maritime forest, and freshwater ponds. The eastern portion of the island has a double-dune structure, and the middle and western parts of the island have relatively lower elevations.

The average annual offshore wave power density in this region is approximately 1.7 kW/m [42]. This wave action, along with the regular occurrence of tropical cyclones, has made Dauphin Island especially vulnerable to coastal erosion. The rate of coastal erosion was estimated as 4.7 m/yr at the beginning of the century [43]. Dauphin Island has undergone substantial morphological changes over the past century due to coastal processes and extreme events, causing breaches and island migrations [44]. Specifically, Dauphin Island has experienced each of the Sallenger storm impact scale categories, i.e., swash, collision, overwash, and inundation [45]. Swash (i.e., when TWL is lower than the dune toe) and collision (i.e., when TWL exceeds the dune toe) regimes can be observed under fair weather conditions across the island. Due to its lower elevation, the western portion of the island has historically experienced the overwash regime (i.e., when water levels gradually increase and exceed the dune crest) and inundation (i.e., when the TWL

exceeds the height of the entire beach system) under storm conditions. On the eastern portion of the island the collision regime is more prevalent due to its higher elevations and double dune structure.

Figure 1. Study location; Dauphin Island, AL. (Created using Google Earth base map).

There have been substantial efforts to protect and stabilize the inhabited eastern and middle portions of Dauphin Island through the construction of groins and breakwaters [43,46]. Dunes have also played an essential role in regulating storm impacts. In the eastern portion of the island, dune heights reaching up to 3 m have been constructed and fortified to defend the homes and infrastructure behind them; however, this region remains subject to significant morphological change. The low elevation of the middle portion of the island makes it particularly susceptible to breaching [47]. During Hurricane Katrina in 2005, a breach was generated in the middle of the island (known as the "Katrina Cut") and has since been restored with rocks, but the area remains vulnerable to substantial wave attack and storm surges. The uninhabited western portion of the island is the most susceptible to collision, overwash, and inundation during storm events due to the low dune heights (less than 1.5 m) and the absence of protective structures. Figure 2 shows the prestorm bed elevations at three cross-shore transects along the island.

2.2. Hurricanes

Dauphin Island has been impacted by ten major hurricanes in the past 25 years. For this study, we focused on simulating the impacts of two major hurricanes that affected Dauphin Island, AL during this time period: Hurricane Ivan and Hurricane Katrina. Hurricane Ivan occurred in 2004 and was one of the most catastrophic storms in U.S. history [48,49]. After peaking in strength, Ivan traveled northward across the GOM and made landfall in Gulf Shores, Alabama as a Category 3 hurricane (Figure 3). It was ultimately responsible for USD 20.5 billion in property damage [48] and 32 confirmed deaths in the United States [49]. Hurricane Katrina made landfall in southeast Louisiana as a Category 3 hurricane (Figure 3); and became the costliest natural disaster in U.S. history

at that time, causing USD 125 billion in property damage [48]. To compensate for the losses, The National Flood Insurance Program funded nearly USD 15 million to insurers in Dauphin Island alone [50]. Katrina was also responsible for 1833 confirmed deaths, including 2 that occurred in Alabama [51].

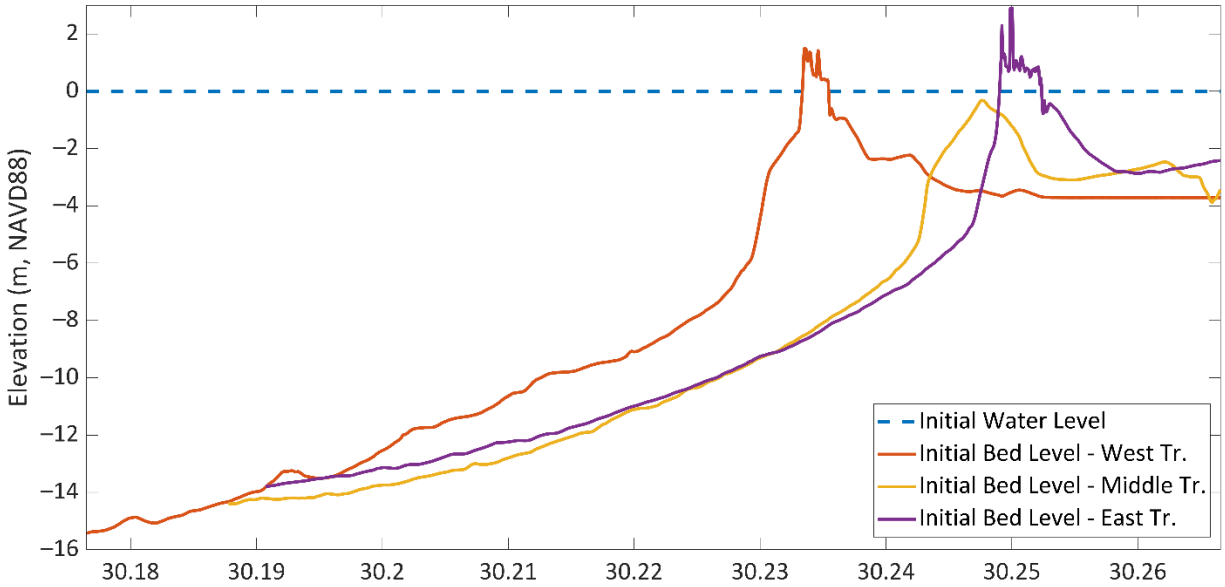

Figure 2. Initial Profiles (Prestorm Bed Levels) and Water Level (dashed line) for west, middle, and east transects of Dauphin Island, AL shown in Figure 4.

2.3. Model Description

XBeach is an open-source, process-based numerical model, and here we use version 1.23.5527 [52]. This model was developed to simulate hydrodynamic and morphodynamic processes and their impacts on sandy coastlines. Specifically, it can simulate wave-induced currents and consequential sediment transport and morphological changes. It simultaneously solves equations defining the short wave-action balance, mass and momentum balance, roller energy balance, nonlinear shallow water flow, sediment transport, and bed update processes [53]. The spatial scale of XBeach can be on the order of several kilometers, and its time scale is on the order of several days, i.e., the duration of a typical severe storm. XBeach resolves the hydrodynamic processes of short and long wave transformation, wave-induced setup, and overwash and inundation across a user-specified grid. Morphodynamic processes, including bedload and suspended sediment transport, bed update and breaching, and dune face avalanching are also resolved. XBeach has successfully modeled hydrodynamics and storm-induced beach and dune evolution in both 1D and 2D on a variety of coastlines [20,24,28,32,54,55], making it a useful tool for investigating the morphological changes induced by the hydrodynamic effects associated with wave farms.

2.4. Model Setup and Assumptions

Here, we use a previously validated two-dimensional model for Dauphin Island [56]. The domain extends approximately 6 km seaward, 3.5 km landward, 3.5 km westward, and 2 km eastward of the island (Figure 4). The alongshore spatial resolution is 25 m, and the variable cross-shore spatial resolution ranges from 12.5 m in the offshore to 3 m across the subaerial island.

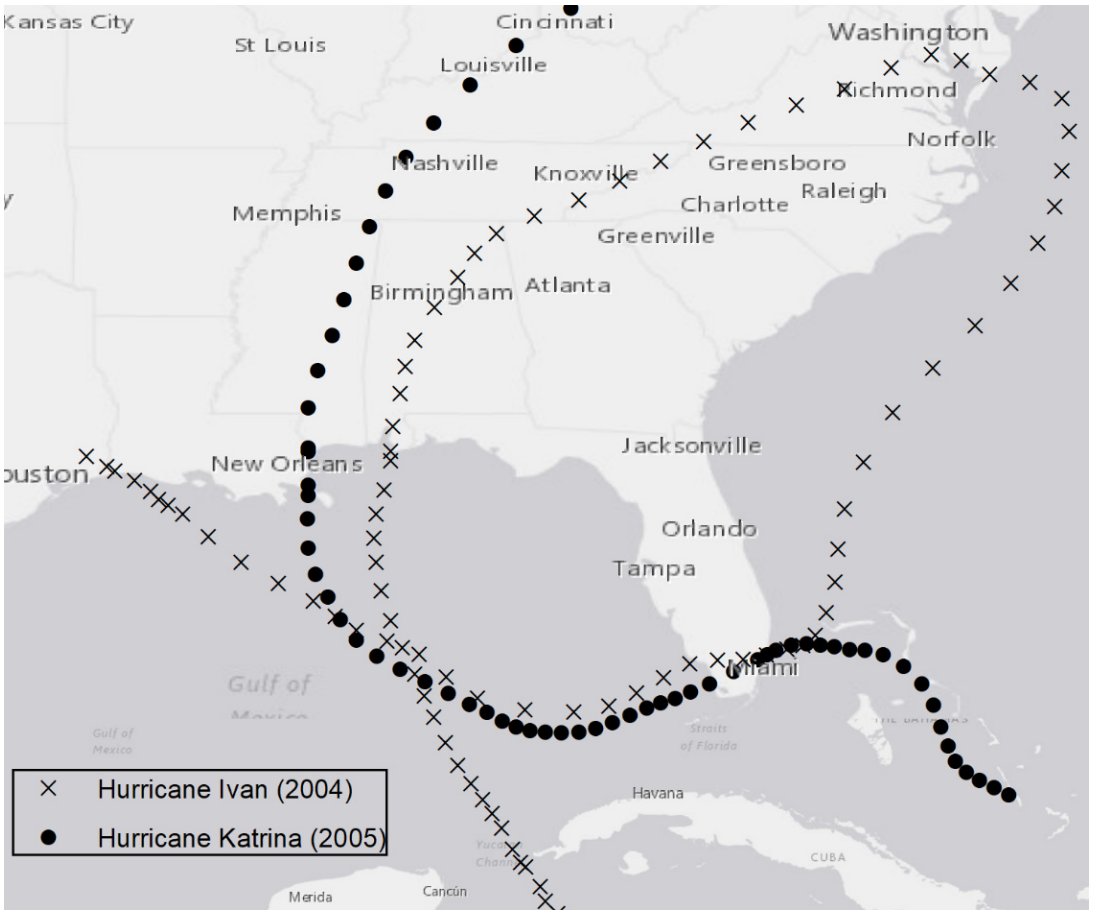

Figure 3. Hurricane Tracks of Ivan and Katrina (Created using ESRI World Topo Base Map).

The topographic and bathymetric data were derived from a post-Katrina digital elevation model [57]. This dataset describes the Katrina Cut, i.e., the breach that occurred in the middle of the island after Hurricane Katrina in 2005 (Figure 4, middle transect). Using this data set allows us to simulate the impacts of Hurricane Ivan and Hurricane Katrina under present-day conditions with and without the wave farm. Bed friction coefficients were parameterized using spatially variable Chezy coefficients based on land use/land cover data [56].

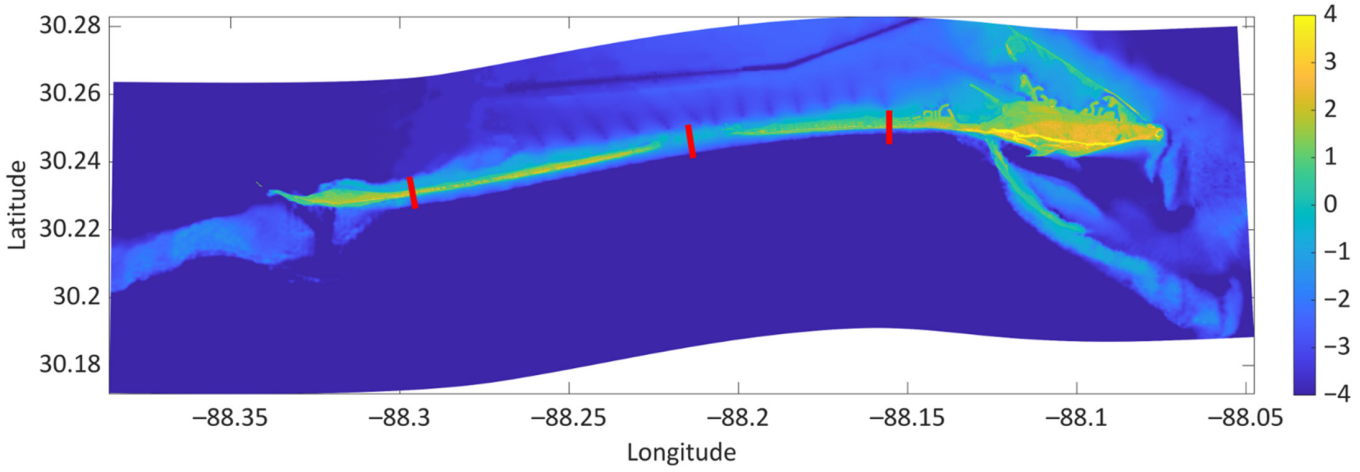

Figure 4. XBeach model domain, presimulation elevations (m, NAVD88), and cross-shore transects (red lines) for Dauphin Island, AL analyzed in this study.

A number of previous studies have used numerical wave models such as Simulating Waves Nearshore (SWAN) to investigate hydrodynamic impacts of WECs, specifically the behavior of the wave climate in the lee of the wave farms. WECs are often represented as partially transmitting and partially reflecting obstacles through transmission and reflection coefficients (K_t and K_r, respectively), which define the ratio of transmitted or reflected wave heights to incident wave heights [58]. These coefficients are specific to individual WEC devices and also the configuration of the wave farm and are generally estimated from laboratory experiments [34,35,59]. Both K_t and K_r range from 0 to 1, where $K_t = 0$ represents complete energy absorption by the WECs (no wave transmission through the WEC farm) and $K_t > 0$ represents partial-to-full wave transmission. Similarly, $K_r = 0$ represents no wave reflection by the WECs, and $K_r > 0$ represents partial-to-full wave reflection [58]. The presence of a wave farm can also be represented through wave parameters, such as wave heights and wave periods, obtained from a wave model, and then used as input to morphological models to investigate the morphological changes caused by WECs [24,32].

In this study, WECs are represented in the XBeach model through adjustments to the offshore boundary conditions, which are extracted from a coupled Advanced Circulation (ADCIRC)+SWAN model [60,61]. A hypothetical wave farm is assumed to be located along the offshore boundary, since the adjustments to boundary conditions are made to the offshore boundary. The XBeach model is forced with JONSWAP (Joint North Sea Wave Project) wave spectra data describing the wave climate (i.e., significant wave heights, peak frequencies, directional spreads, and main wave angles) and time-series water levels derived from a large-scale ADCIRC+SWAN model that has been validated for Hurricane Ivan and Hurricane Katrina [60]. A time-series of JONSWAP spectra is applied uniformly along the offshore boundary. Time-series of hourly water levels are forced uniformly across the onshore and offshore grid boundaries for Hurricane Ivan. For Hurricane Katrina, water levels are forced at the four corners of the XBeach grid [56]. The XBeach model is executed in surfbeat (instationary) mode to develop the baseline scenario (i.e., the case without WECs). Wave heights in the JONSWAP spectra range between 0.76m and 5.55 m for Hurricane Ivan, and 0.65 m and 5.99 m for Hurricane Katrina. Wave frequencies range between 0.0492 s^{-1} and 0.1674 s^{-1} for Ivan, and 0.0628 s^{-1} and 0.2332 s^{-1} for Katrina. Hurricane Ivan is simulated for 63 h, and Katrina is simulated for 91 h based on the available data and duration of the storms. Directions (i.e., main angle) of the storms following the storm tracks are shown in Figure 3.

Next, the significant wave heights are reduced by 30% for the wave farm scenario. This reduction is chosen based on recent studies on the efficiency of various types of WECs including overtopping devices and point absorbers, which indicate that 30% is a conservative but reasonable reduction ([24,25]). The reduced significant wave heights along with the same water levels, wave directions, and peak wave periods from the baseline scenario are then input to the XBeach model. The model is run for both scenarios, and differences between the two cases are investigated. The impacts of the wave farm on the morphology, water levels, and nearshore wave climate are observed. Specifically, the peak and total water levels, regimes (e.g., collision, overwash, etc.), wave heights, dune heights, bed elevations, inundated area, and bed shear stresses are used as proxies to assess the differences between baseline and wave farm scenarios. With this approach, physical wave-to-WEC or WEC-to-WEC interactions are not captured, i.e., we only represent the energetic effects of wave farms. It should also be noted that since the waves are forced on the offshore boundary, the effects of any localized wind waves are not resolved, i.e., we are only assessing the effects of the wave farm on the offshore waves that propagate landward. Nevertheless, this serves as a fundamental step in understanding the (minimum) potential of WECs to reduce coastal erosion; including physical effects would likely cause additional reduction.

3. Results

3.1. Hurricane Ivan

3.1.1. Response of Water Levels and Nearshore Wave Climate to Simulated Wave Farms

Here, we compare the output of the baseline (i.e., significant wave heights (Hs) unchanged) and wave farm (Hs reduced by 30%) simulations to assess the impact of WECs. Peak water levels during Hurricane Ivan, and the pre- and post-storm bed levels for the baseline and wave farm scenarios are presented in Figure 5. The TWL exceeds most dune heights and inundates a significant portion of the island in both the baseline and wave farm scenarios. Peak water levels evaluated at the beach face for the baseline scenario are higher than those observed in the wave farm scenario along the west and middle transects, by 0.3 m and 0.1 m, respectively (Figure 5a,b). Along the east transect, however, the peak offshore water level in the wave farm scenario (where the Hs is lower) is ~0.5 m higher than that in the baseline scenario, and overtops the primary dune causing erosion with sand deposited in the nearshore (Figure 5c). This is in contrast to the baseline scenario, where the collision regime is observed at the primary dune, which causes avalanching. This is likely due to nonlinear superposition of swell waves and wind waves, which can create higher TWL at irregular locations [62,63]. Additionally, the impact of the reduction in wave heights due to WECs on TWL varies in the north–south direction, as the hydrodynamics are also influenced by the bottom surface (i.e., friction and topography) and geometry of the island. This illustrates that the TWL is not always directly related to the wave heights defined on the offshore boundary. In other words, the role of WECs in potentially changing the TWL or the regime varies across the coast. The maximum water levels reached at each grid cell during the simulation for the baseline and wave farm scenarios, as well as the difference between the two scenarios, are illustrated in Figure 6. Overall, lower maximum water levels are observed in the wave farm scenario (Figure 6b) compared to those observed in baseline scenario (Figure 6a). The difference in maximum water elevation of the two model scenarios illustrates the alongshore variability in maximum TWLs; the wave farm scenario has high water levels compared to the baseline scenario near the eastern portion of Dauphin Island (Figure 6c). Conversely, the opposite is illustrated for the western portion; therefore, it should not be assumed that reduced wave heights offshore will result in uniformly lower total water levels across the whole domain. For this storm, the wave farm is more effective in reducing the TWL in the western part of the island where the water levels are the highest in both the baseline and wave farm scenarios, which may have implications for the ideal configuration of wave energy converters to achieve similar efficacy in the eastern region. Additionally, this may mean that WECs make a bigger impact on the areas with high maximum water levels. Focusing on the western portion of the island, Figure 6d,e shows that the dry areas are more prevalent in the wave farm scenario than the baseline, indicating that the presence of wave farms reduces overtopping and inundation at this location.

We examine how WECs impact wave-induced erosion by analyzing the maximum Hs across the domain in both scenarios (Figure 7). It is observed that the Hs is lower for the wave farm scenario relative to the baseline, as is expected due to the adjustment in Hs on the offshore boundary condition to represent the wave farm. On average, the nearshore wave heights in the wave farm scenario were found to be 0.3 m lower than the baseline scenario, which results in lower potential erodibility due to decreased wave action (Figure 7c). There are some areas where the wave farm does not make any impact, i.e., the white areas, which indicates the same Hs for both scenarios. Additionally, Hs in the wave farm scenario appears to be slightly higher in the east and west portions of the island compared to the baseline scenario, indicating that the impact of WECs on wave height is reversed in the sheltered areas (east of the island) and landward of breaches. Figure 7c illustrates that the impacts of WECs on Hs are not uniform, and we see pockets of no differences due to the complex hydrodynamics. We mostly see no change in Hs behind the island, with the exception of the Katrina Cut; here we again see higher wave heights in the wave farm scenario, likely due to the channeling discussed in Section 3.1.2. In Figure 7d, the percent difference in Hs is presented, and although the wave heights at the offshore

boundary are reduced by 30% to represent the wave farm, this percent change does not remain constant as waves propagate to the coast. In some areas, wave height reduction reaches 50% (indicated by a circle in Figure 7d) in the wave farm scenario. This suggests that the impacts of a wave farm on Hs extend beyond its local circumference (i.e., the offshore boundary in this case).

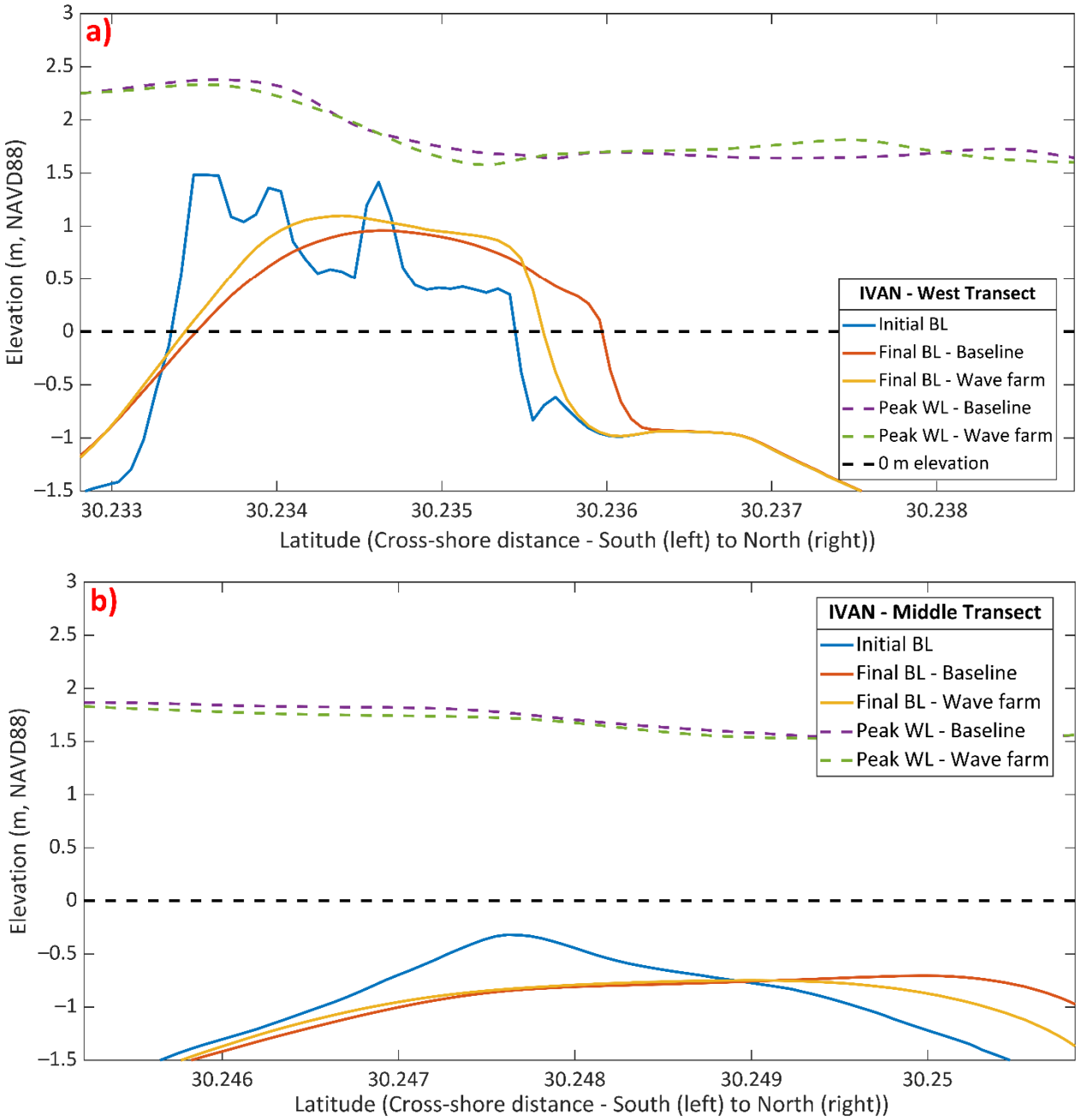

Figure 5. *Cont.*

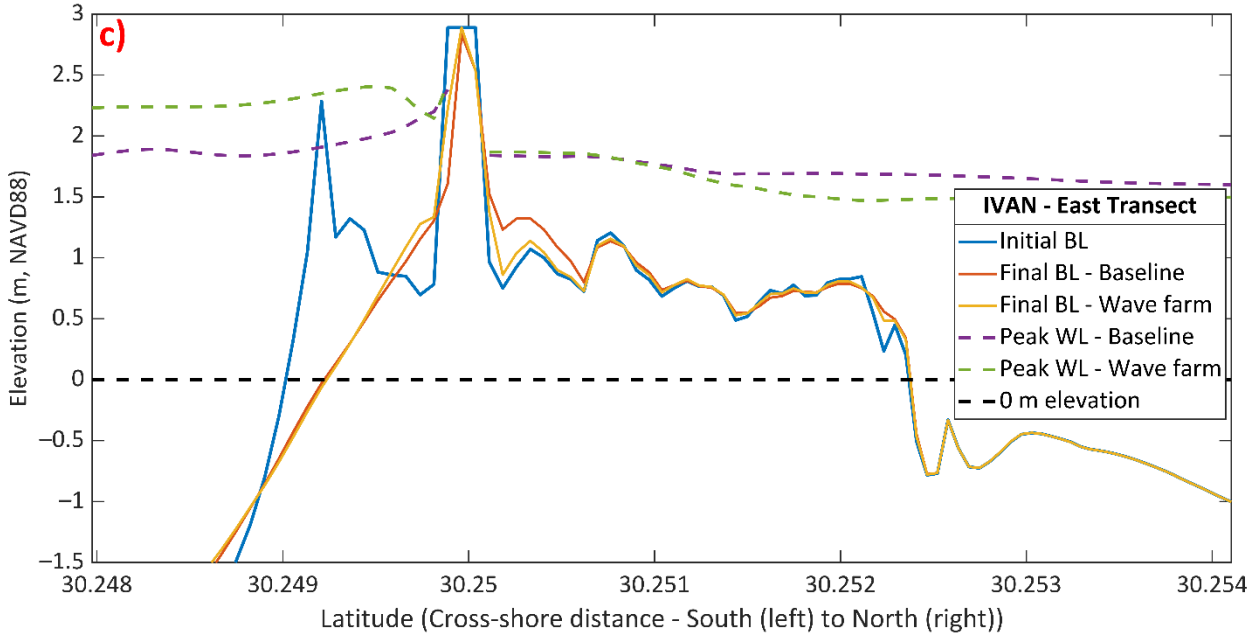

Figure 5. Hurricane IVAN bed levels (BL) and water levels (WL) at the west (**a**), middle (**b**), and east (**c**) transects on Dauphin Island, AL under baseline and wave farm scenarios. Note that the figures are zoomed in for readability. Initial WL is at the zero level for all transects.

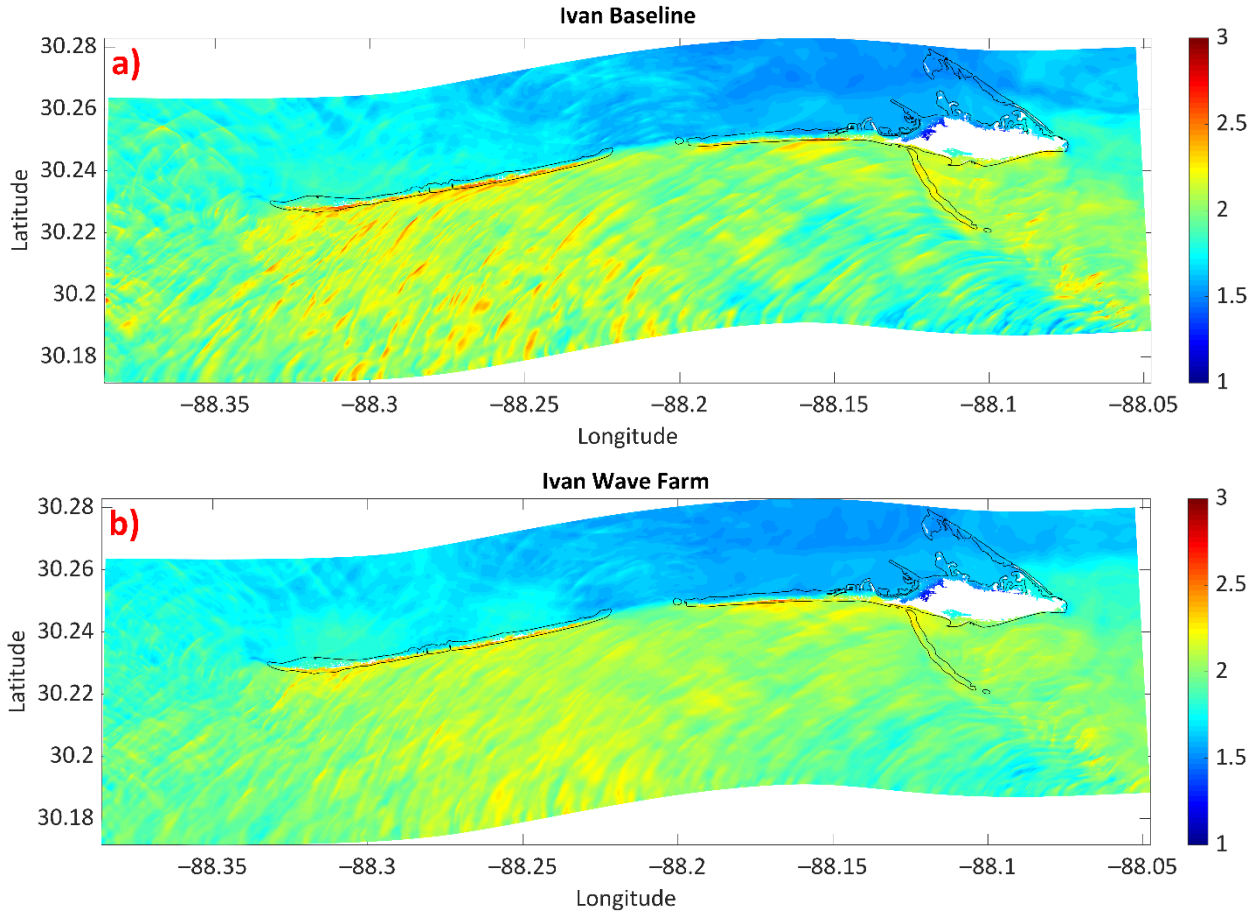

Figure 6. *Cont.*

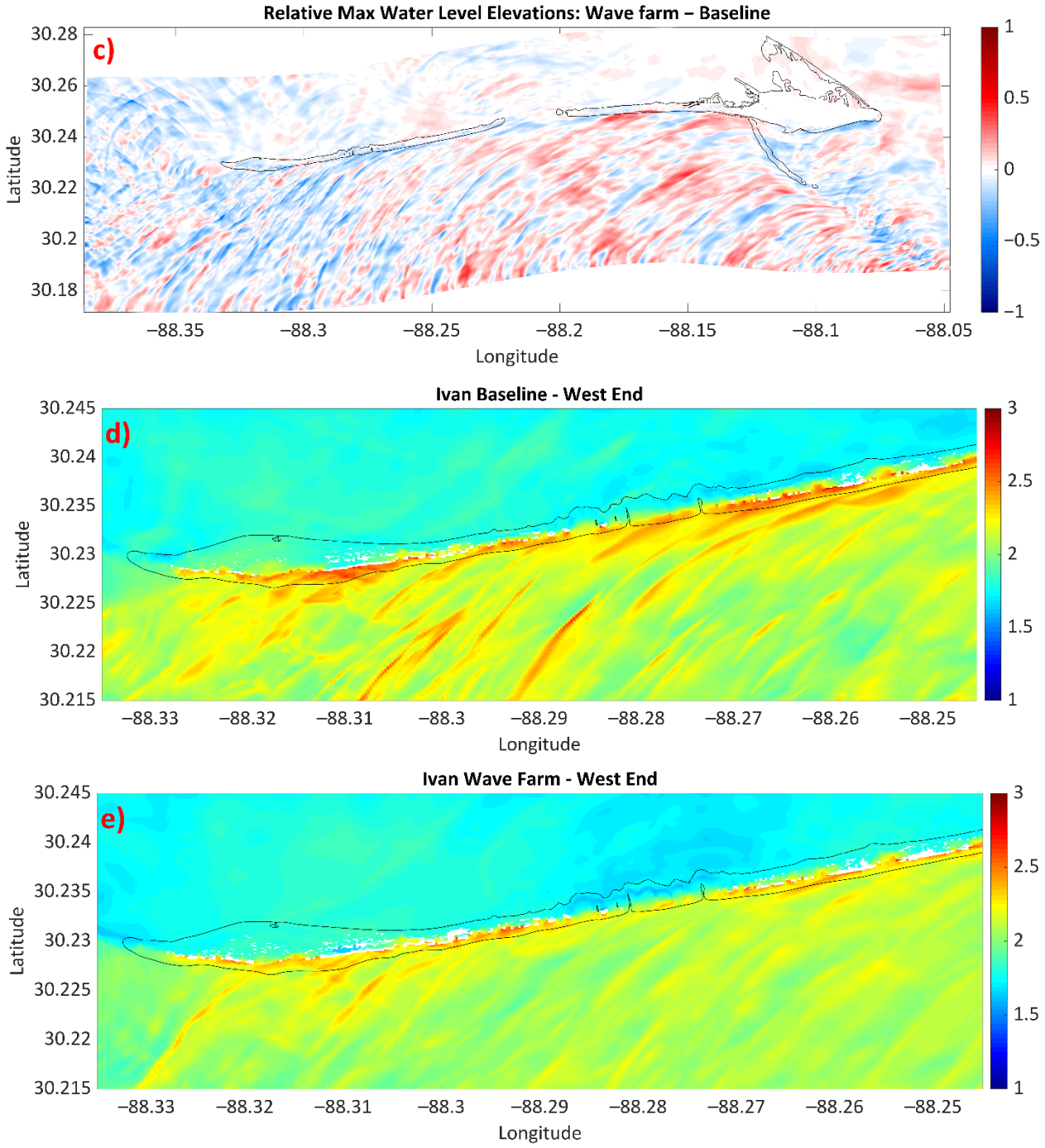

Figure 6. Maximum water levels [m] for baseline (**a**) and wave farm (**b**) scenarios for Dauphin Island, AL. (**c**) Difference between the two scenarios: (**b**) subtracted from (**a**). (**d**,**e**) Magnified versions of (**a**) and (**b**), respectively. White patches are the dry areas, and the black line is the poststorm zero-meter contour of the island.

3.1.2. Response of Morphology to Simulated Wave Farms

To relate the impacts of water levels to coastal morphology, we examine the dune heights, bed elevations, inundated area, and bed shear stress across the island. Initial and final beach profiles are extracted from transects located on the eastern, middle, and western regions of the island (Figure 4). Morphologic changes to the beach, dune face, and dune heights are used as proxies for coastal erosion and bed level change.

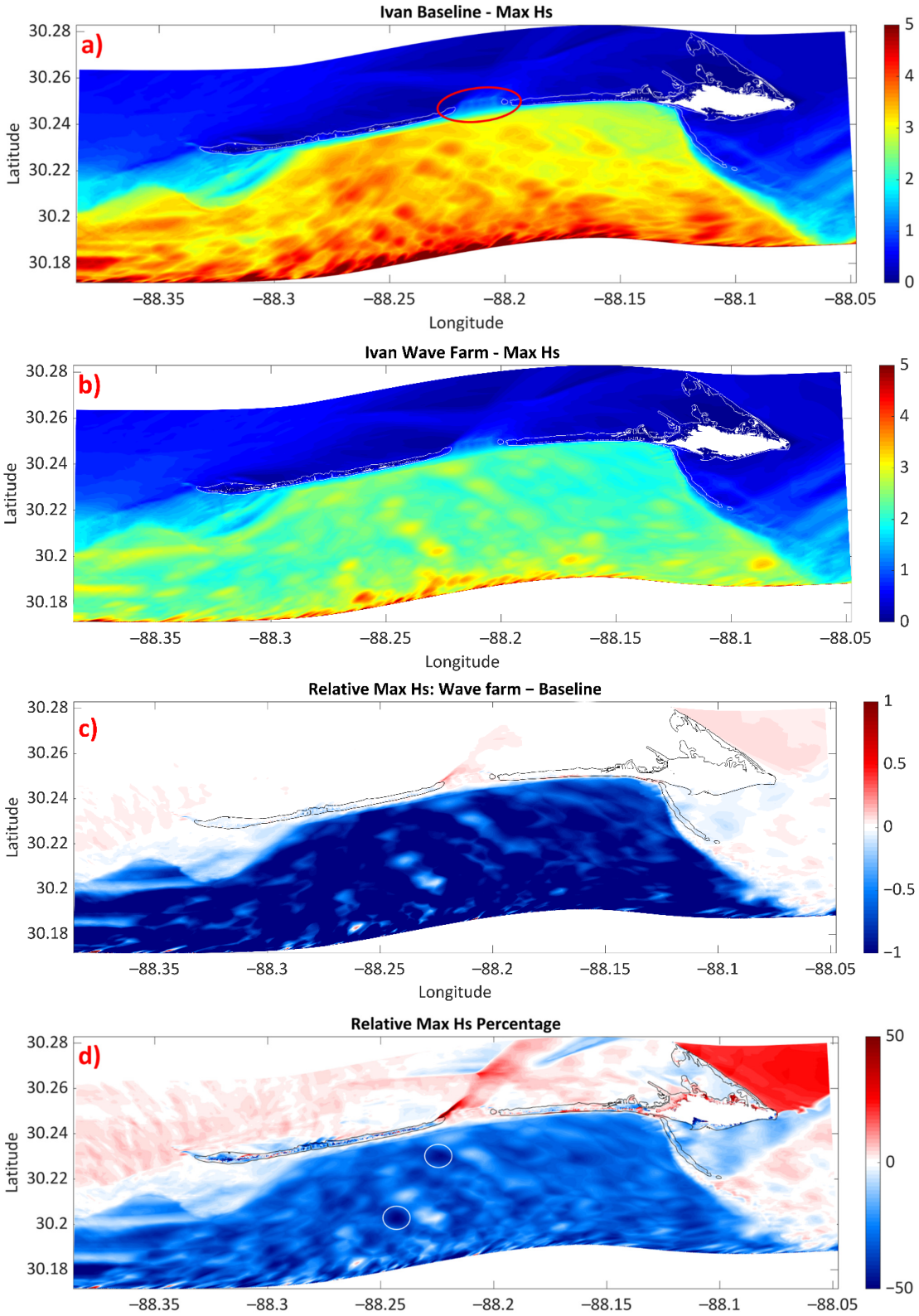

Figure 7. Hurricane Ivan maximum wave heights (Hs) across the domain of Dauphin Island, AL: (**a**) baseline scenario [m], (**b**) wave farm scenario [m] (**c**) Hs difference between the two scenarios in [m] where baseline values are subtracted from wave farm values. (**d**) Hs difference in [%]. White circles are some of the locations where the reduction in Hs exceeds 50% in the wave farm scenario. The blue color represents the reduction in Hs due to wave energy converter devices (WECs), and the red color represents the increase in Hs due to WECs. White and black lines are the poststorm zero-meter contours of the island. The location of the Katrina Cut is marked with a red circle in (**a**).

The average dune crest heights across the island are 3.24 m and 3.33 m for the baseline and wave farm scenarios, respectively. This shows a 3% reduction in the dune loss across the island with the presence of WECs. The maximum dune height difference between the two scenarios occurs at 825 m west of the west transect, where the dune height in the wave farm scenario is 1.77 m higher than in baseline scenario (see Figure 8). These results illustrate how wave dampening by wave farm presence can help diminish the damage due to inundation and overtopping.

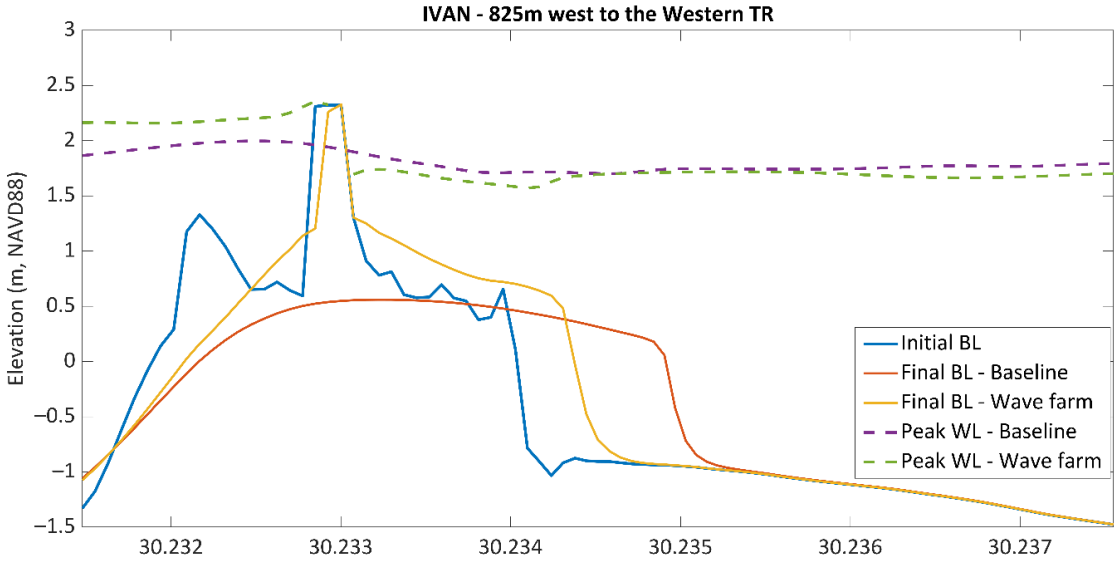

Figure 8. Hurricane Ivan bed levels (BL) and water levels (WL) under baseline and wave farm scenarios at the location on Dauphin Island, AL where the maximum dune height difference between the two scenarios occurs.

We also investigate the changes in the dune heights and beach profile at the west, middle, and east transects, shown in Figure 4 to better understand the morphological response in different regions of the island. At the west transect (Figure 5a), the inundation caused by Hurricane Ivan causes sediment to be mobilized at the dune face and deposited behind the dune structure in the baseline scenario, and the dune height is reduced by 0.75 m. In the wave farm scenario, the dune height is only reduced by 0.5 m, i.e., the erosion is mitigated by 33% when the hydrodynamic impacts of wave farms are represented. The differences in dune heights in the two scenarios are not as pronounced for the middle and east transects. The middle transect is located at the breach of the island (i.e., it is initially underwater); therefore, the changes in the surface wave heights do not substantially alter the underwater bathymetry (Figure 5b). The east transect is prevented from complete inundation by the high double-dune structure (Figure 5c). The primary dune takes on the impacts of the storm and is eroded, while the secondary dune stays intact in both scenarios. The difference between the final dune heights in the two scenarios is not substantial, most likely due to the wave action being dissipated by the first dune and the high water levels dominating the erosion process in the second dune. However, the height of the second dune is slightly (5.5 cm) higher in the wave farm scenario in contrast to the baseline scenario. For both scenarios, the bed elevations are unchanged from the initial (prestorm) profile in both the seaward and landward ends of the transects. At all three transects and for both scenarios, the sediment in the beach face is transported and deposited onshore poststorm (i.e., immediately behind the prestorm dunes), creating irregular and shallow sand dunes. Figure 5a–c show that in the baseline scenario, the sediment is transported 5 to 50 m further inland than in the wave farm scenario for all three transects, i.e., the Final BL-Baseline curve appears 5 to 50 m north (towards the land) of Final BL-Wave farm curve, at all three transects.

The differences in the final bed elevations across Dauphin Island post-Ivan under the baseline and wave farm scenarios are shown in Figure 9. On the western portion of the island, higher accretion in the westernmost point and lower cross-shore sediment transport are observed in the presence of the wave farm compared to the baseline scenario. Additionally, there are fewer channels cut through the island in the wave farm scenario (Figure 9d). This substantially reduces the breaching tendencies in the area where the island is the narrowest, with a width of ~230 m. In Pelican Island and the middle breach, however, slightly lower bed elevations (i.e., more erosion) are observed in the wave farm scenario. This can likely be attributed to the dominant swell wave angle coming from the southeast (SE 144.05°), which causes the sediment to be transported to the west [64]. The middle breach shifts westward in the presence of the wave farms, and the width is 200 m smaller than in the baseline scenario (the breach width is 2.4 km in the baseline scenario and 2.2 km in the wave farm scenario). A smaller breach opening and lower bed levels underwater in the presence of WECs indicate that wave farms can cause more precise erosive action at a breach.

To quantify the impacts of the wave farm on coastal sediment, we present the results of the inundated area, volume loss, and bed shear stress calculations for both scenarios in Table 1. The initial area and volume of the island are identified by determining the dry and wet cells within the computational domain. The zero-meter contour is identified, and initial area and volume values are calculated based on the cells that fall into the zero-meter polygon. Maximum water levels that occurred throughout the simulation are determined for each cell, and they are compared to the initial and final bathymetry (i.e., z-value) to determine the inundated cells for volume loss calculations. We find that the poststorm subaerial island area and subaerial sand volume are higher when the WECs are present. Additionally, the total inundated area and net loss in the sand volume are lower in the wave farm scenario. Results indicate a 15% reduction in the net loss of sand volume due to the wave farm.

Table 1. Inundated and dry areas, initial and final sand volume, net loss in sand volume, and maximum bed shear stress values in x- and y-directions [N/m^2] averaged over time in the mid-domain nearshore area of Dauphin Island, AL under Hurricane Ivan conditions for baseline and wave farm scenarios.

IVAN	Baseline	Wave Farm	Difference
Initial island area (millions of m^2)	14.19	14.19	-
Total dry area (millions of m^2)	4.49	4.59	2%
Total inundated area (millions of m^2)	9.69	9.59	−1%
Initial sand volume (millions of m^3)	19.73	19.73	-
Final sand volume (millions of m^3)	19.00	19.10	0.5%
Net loss in sand volume (millions of m^3)	0.73	0.62	−15%
Maximum τ_{bx}	192.24	118.69	−38%
Maximum τ_{by}	76.19	67.81	−11%
Maximum $\tau_b = \sqrt{{\tau_{bx}}^2 + {\tau_{by}}^2}$	206.79	144.71	−30 %

Bed shear stress is used as another indicator of erosion at the bed level, as the likelihood of ocean bottom sediment to be mobilized is directly correlated with the intensity of bed shear stress [40,65]. XBeach calculates the bed shear stress associated with the long waves and mean currents using the following formulation in the cross-shore; x-(τ_{bx}) and alongshore; y-(τ_{by}) directions [53]:

$$\tau_{bx} = c_f \rho u_E \sqrt{(1.16\, u_{rms})^2 + (u_E + v_E)^2} \quad (1)$$

$$\tau_{by} = c_f \rho v_E \sqrt{(1.16\, u_{rms})^2 + (u_E + v_E)^2}, \quad (2)$$

where c_f is the dimensionless friction coefficient, ρ is the density of water, u_E, and v_E are the Eulerian east–west and north–south velocities, respectively, and u_{rms} is the root-mean-square velocity. In this study, the average maximum bed shear stress in the x- and y-directions over the duration of the storm in the mid-domain nearshore area (i.e., where the water depths are low and bed shear stress is responsive to the changes in the wave heights) is calculated. The maximum shear stress in the wave farm and baseline scenarios, as well as the differences between them, are listed in Table 1. The maximum averaged bed shear stress values are reduced from 206.79 to 144.71 N/m^2 for the baseline and wave farm scenarios, respectively (30% reduction). It is observed that the reduction in the y-direction (alongshore; 11%) is lower than the reduction in the x-direction (cross-shore; 38%), indicating that the presence of wave farms impacts the bottom sediment transport more in the cross-shore direction than in the alongshore direction.

3.2. Hurricane Katrina

We repeat the methodology described in Section 3.1 with storm data from Hurricane Katrina.

3.2.1. Response of Water Levels and Nearshore Wave Climate to Simulated Wave Farms

Results of the simulations of Hurricane Katrina show patterns similar to those seen for Hurricane Ivan in terms of the water levels and inundation/overwash regimes experienced along the transects, with the west and middle transects being entirely inundated. However, Hurricane Katrina was a stronger storm and also coincided with high tides, causing peak water levels to exceed 3.5 m and inundate the eastern portion of the island in contrast to the impacts of Hurricane Ivan. Peak water levels are observed to be consistent between the baseline and wave farm scenarios (Figure 10). This indicates that wave farms are not as effective in changing the regime (e.g., collision, overwash) during intense storms when TWL is high.

Figure 11 illustrates the maximum water levels across the domain for both scenarios and the difference between them. As discussed in the case of Hurricane Ivan, Figure 11 indicates overall lower maximum water elevations in the wave farm scenario. In Figure 11c, the areas where maximum TWLs are lower in the wave farm scenario are dominant across the domain, unlike the Ivan case (see Figure 6c). It should be noted that the difference between the TWLs for the two scenarios is on the order of centimeters for Katrina; therefore, it may be inaccurate to conclude that the wave farm is more effective in reducing the TWL across the domain for the Katrina case.

As expected, the maximum Hs is lower in the wave farm scenario compared to the baseline scenario due to the adjustments made in Hs at the offshore boundary to represent the wave farms (Figure 12). The response of the Hs to this adjustment dissipates as the waves propagate towards the shore. On average, the nearshore wave heights in the wave farm scenario are found to be ~0.2 m lower than the baseline scenario.

3.2.2. Response of Morphology to Simulated Wave Farms

The impacts of WECs on dune heights, bed elevations, and beach profiles shown in the Hurricane Katrina case study are similar to those observed with Hurricane Ivan. Hurricane Katrina fully erodes the dune systems at all three transects; however, like Hurricane Ivan, the final bed levels are generally higher in the wave farm scenario than the baseline scenario (Figure 10). The discussion in Section 3.1.2 related to the complete beach profiles and the dune heights across the island under Hurricane Ivan conditions are applicable for the results of the Hurricane Katrina case, i.e., the bed elevations are unchanged from the initial (prestorm) profile in both the seaward and landward ends of the transects, and the sediment at the beach face is transported and deposited onshore poststorm further inland in the baseline scenario at all three transects. The average of subaerial dune heights across the island is found to be 2.46 m and 2.55 m for the baseline and wave farm scenarios, respectively. The maximum dune height difference between the two scenarios occurs at the

eastern end of the island, where the dune height in the wave farm scenario is 1.6 m higher than that observed in the baseline scenario (see Figure 13).

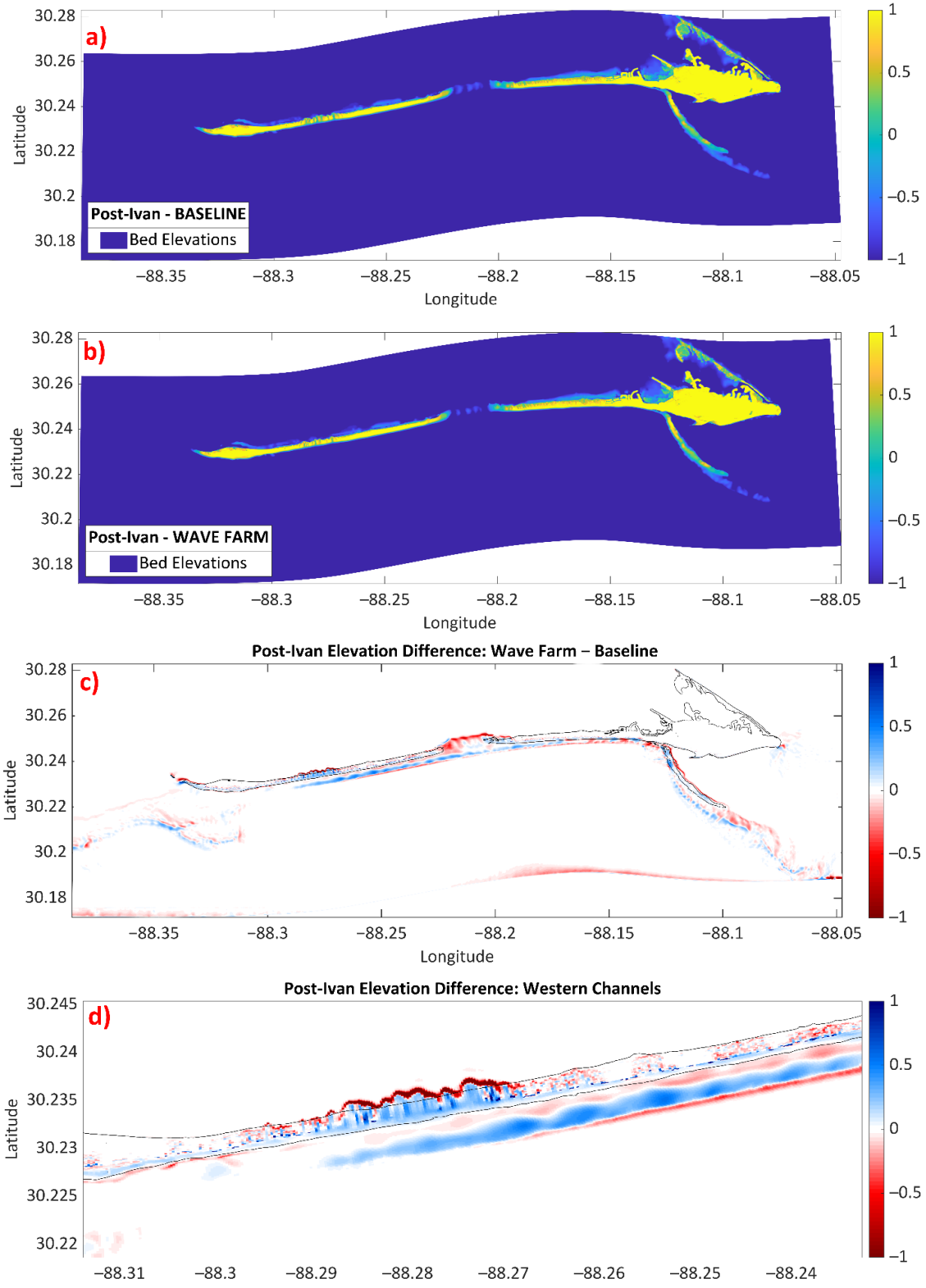

Figure 9. Final bed elevations [m] for baseline (**a**) and wave farm (**b**) scenarios on Dauphin Island, AL. (**c**) Difference between the two scenarios. (**d**) Magnified version of (**c**) showing the channels in the western portion—Positive (blue) values show the locations where the final elevations are higher in the wave farm scenario. The black line is the poststorm zero-meter contour of the island.

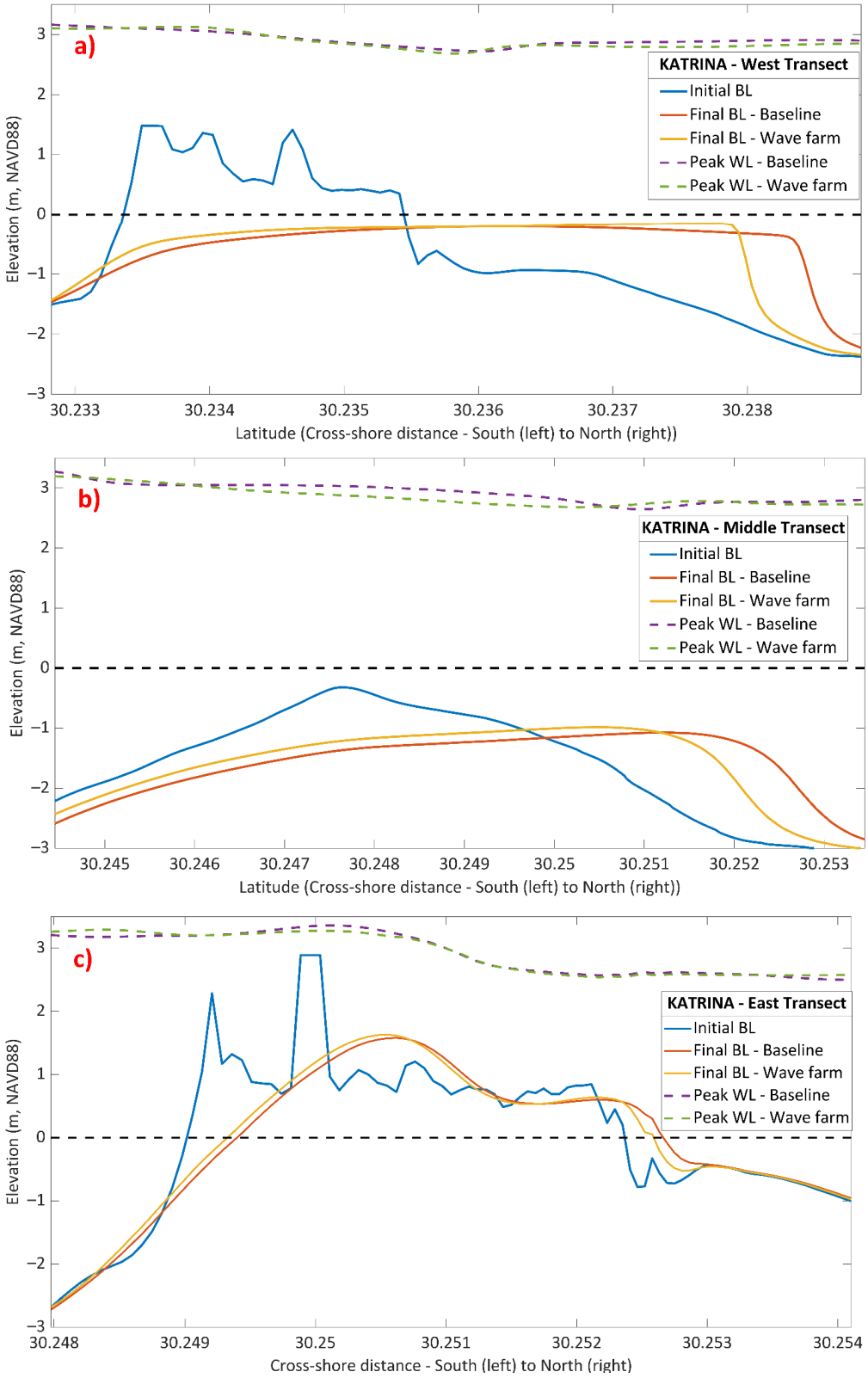

Figure 10. Hurricane Katrina bed levels (BL) and water levels (WL) at the west (**a**), middle (**b**), and east (**c**) transects on Dauphin Island, AL under baseline and wave farm scenarios. Note that the figures are zoomed in for readability. Initial WL is at the zero level for all transects. Black dashed line shows the 0 m elevation.

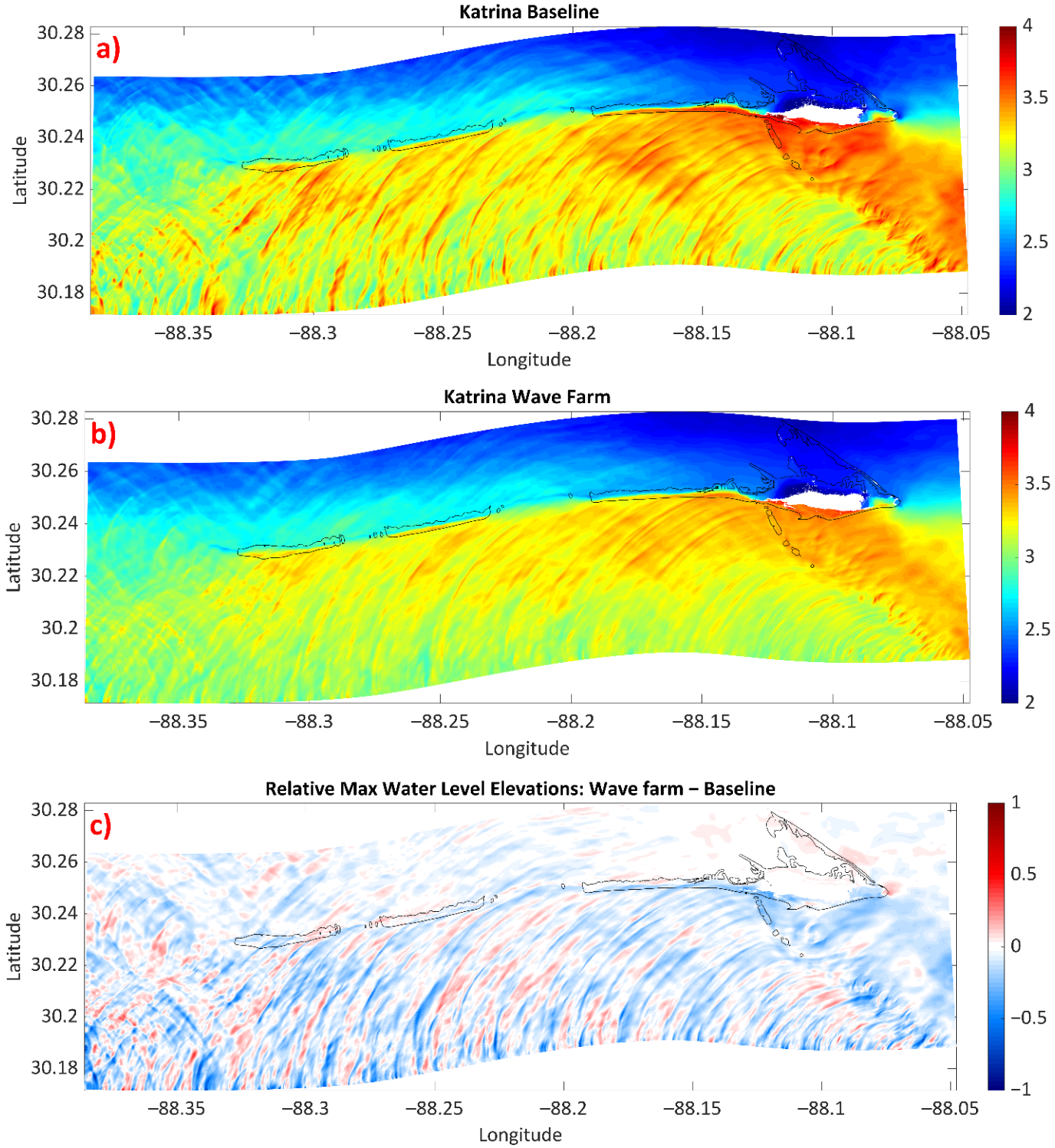

Figure 11. Maximum water levels [m] for baseline (**a**) and wave farm (**b**) scenarios at Dauphin Island, AL under Hurricane Katrina conditions (**c**) Difference between the two scenarios: (**b**) subtracted from (**a**). The black line is the poststorm zero-meter contour of the island.

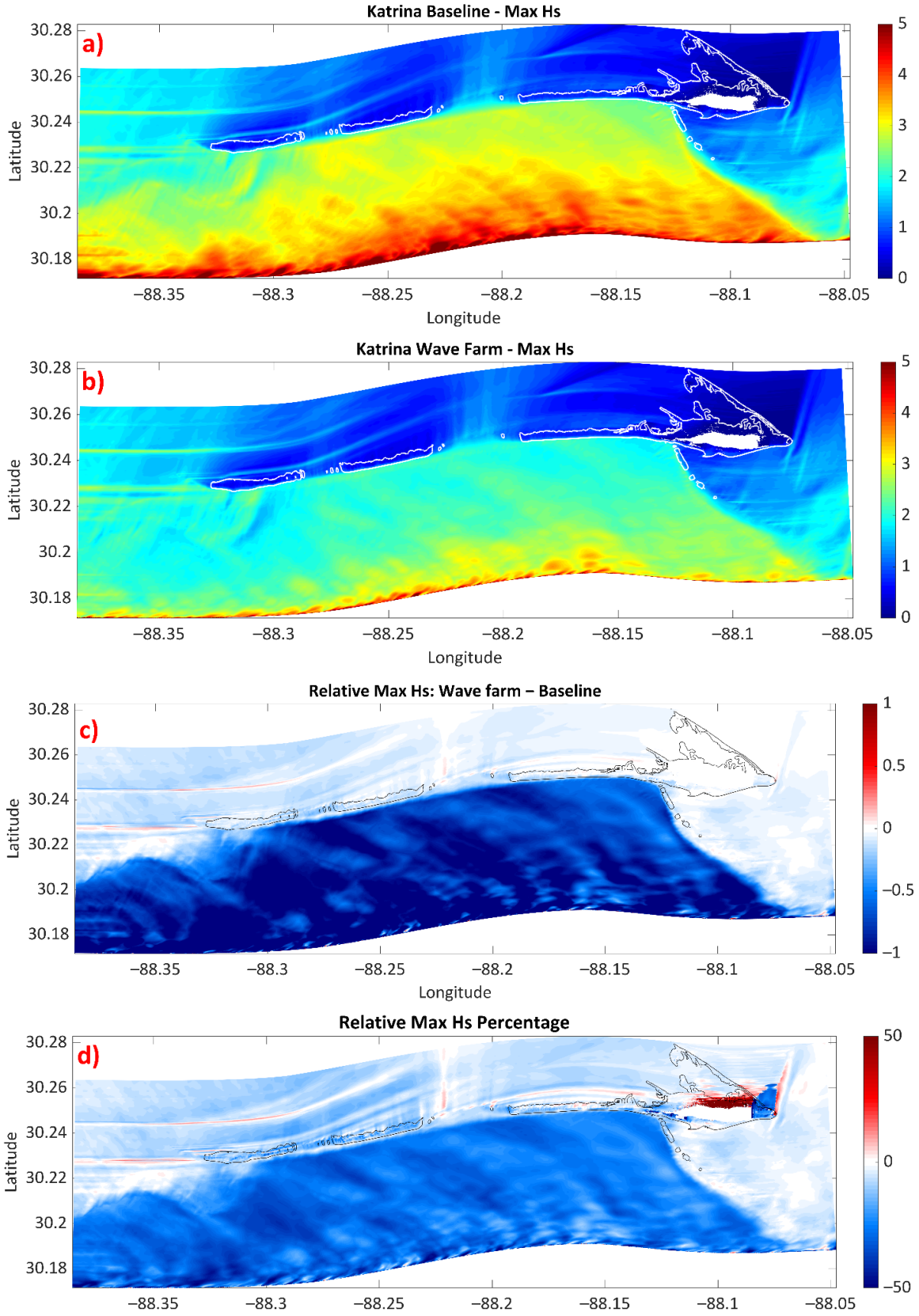

Figure 12. Maximum wave heights (Hs) across the domain of Dauphin Island, AL: (**a**) baseline scenario, (**b**) wave farm scenario. (**c**) Hs difference between the two scenarios in [m] Baseline values are subtracted from wave farm values. The blue color represents the reduction in Hs due to wave energy converter devices (WECs), and the red color represents the increase in Hs due to WECs. (**d**) Hs difference in [%].

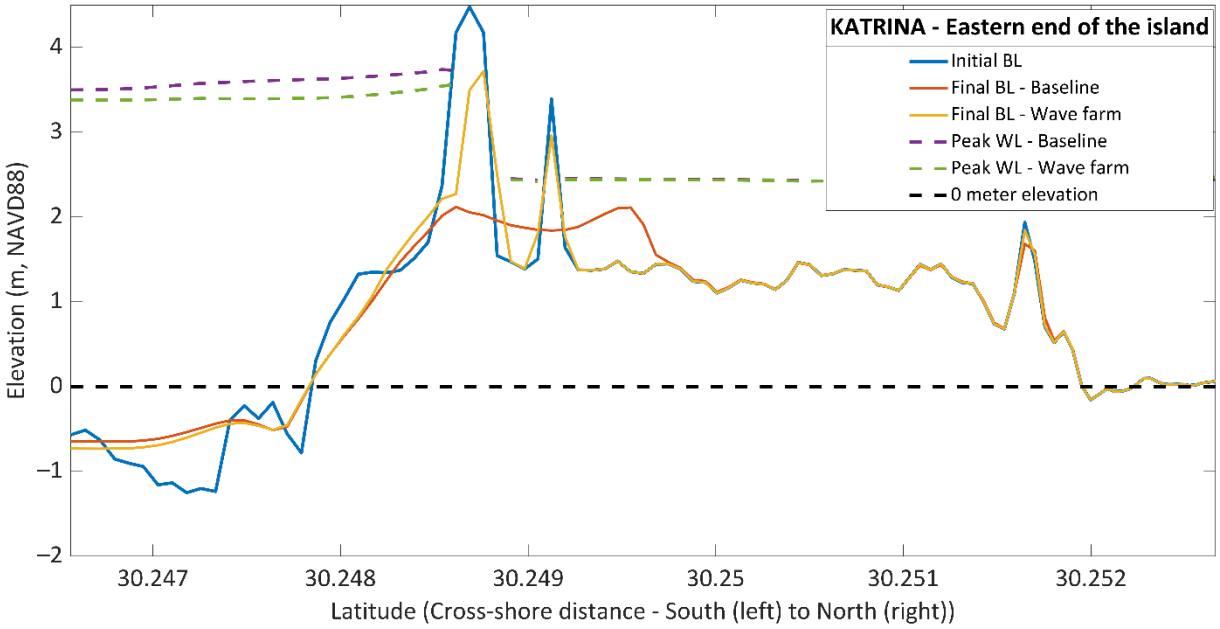

Figure 13. Bed levels (BL) and water levels for Dauphin Island, AL under Hurricane Katrina conditions for baseline and wave farm scenarios at the location where the maximum dune height difference between the two scenarios occurs.

Figure 14 shows the bed levels post-Katrina, where a second breach is observed in the western portion of the island in both scenarios. The difference between the two scenarios is not as pronounced as the Ivan case; however, we observe more landward overwash deposition in the baseline scenario. Even though the dunes are still being overwashed, the wave farm is reducing cross-barrier sediment transport.

Impacts of WECs on the inundated area and volume loss are found to be similar to those seen in Hurricane Ivan, i.e., more dry areas and less sand volume loss are seen with the presence of WECs (Table 2) In the wave farm scenario, the island experiences less inundated area and an 11% reduction in net loss of sediment volume compared to the baseline scenario. Compared to the Ivan case, the difference between the two scenarios is less substantial.

Table 2. Inundated and dry areas, initial and final sand volume, net loss in sand volume, and maximum bed shear stress values in x- and y-directions [N/m^2] for Dauphin Island, AL averaged over time in the mid-domain nearshore area for Hurricane Katrina under baseline and wave farm scenarios.

KATRINA	Baseline	Wave Farm	Difference
Initial island area (millions of m^2)	14.19	14.19	-
Total dry area (millions of m^2)	1.88	1.92	2%
Total inundated area (millions of m^2)	12.31	12.27	−0.3%
Initial sand volume (millions of m^3)	19.73	19.73	-
Final sand volume (millions of m^3)	17.86	18.07	1%
Net loss in sand volume (millions of m^3)	1.87	1.66	−11%
Maximum τ_{bx}	295.03	224.38	−24%
Maximum τ_{by}	106.77	99.30	−7%
Maximum $\tau_b = \sqrt{{\tau_{bx}}^2 + {\tau_{by}}^2}$	313.76	245.37	−22%

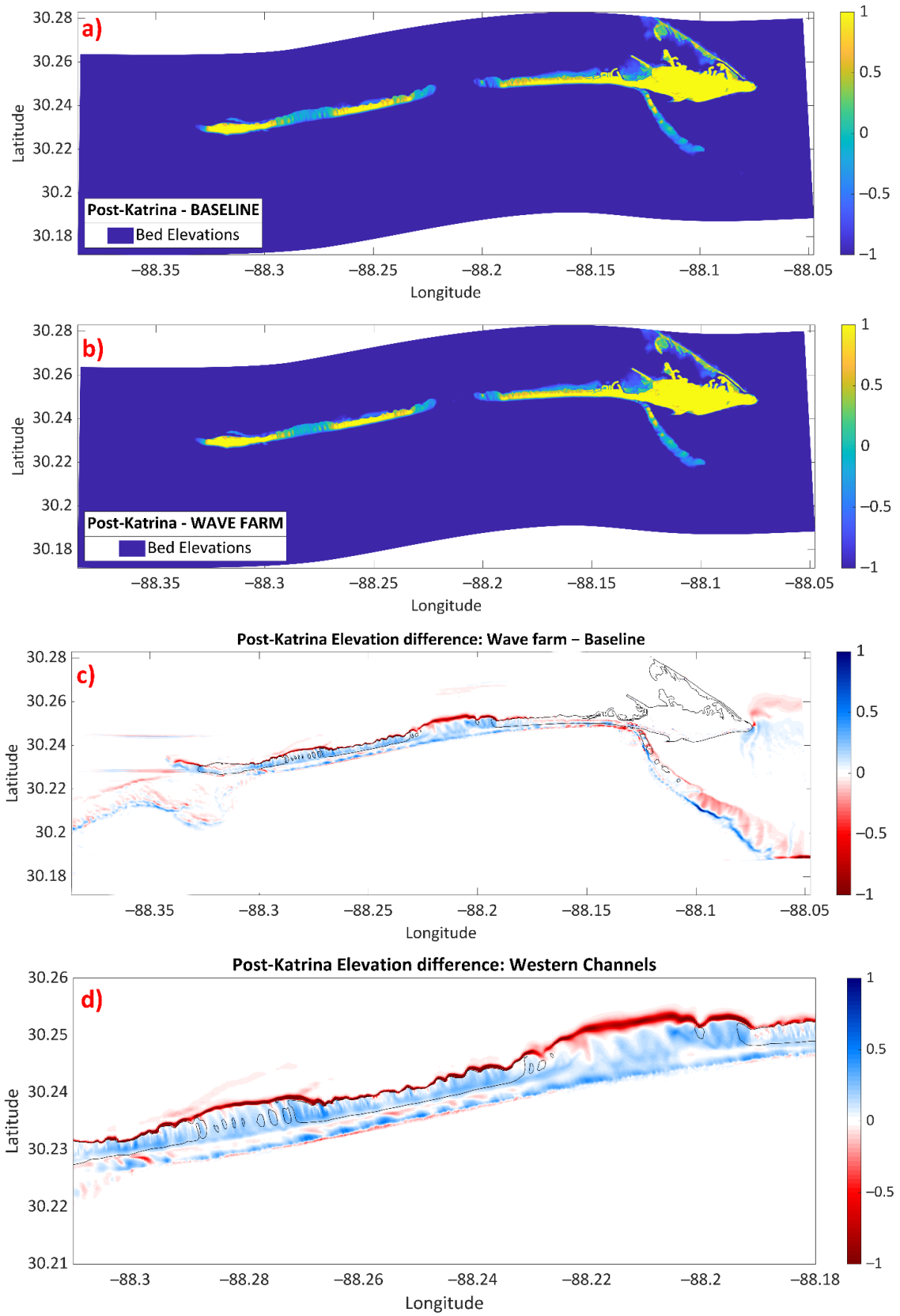

Figure 14. Final bed elevations at Dauphin Island, AL under Hurricane Katrina conditions for baseline (**a**) and wave farm (**b**) scenarios. (**c**) Difference between the two scenarios. (**d**) Magnified version of (**c**) showing the channels in the western portion—Positive (blue) values show the locations where the final elevations are higher in the wave farm scenario. Black lines are the poststorm zero-meter contours of the island.

Finally, the results show that the bed shear stress values are reduced from 313.76 to 245.37 N/m^2 in the presence of a wave farm, indicating a smaller likelihood of the mobilization and erosion of bottom sediment (Table 2). This likely explains why we see less cross-barrier sediment transport in the wave farm scenario (Figure 14c,d).

4. Discussion

Numerical simulations developed to investigate the impacts of a wave farm on coastal morphology under storm conditions show that overall there are lower TWL and maximum Hs, less overwash, less inundated area, less sand volume loss, and lower bed shear stress magnitudes in the wave farm scenario, compared to the baseline scenario. However, the reduction of storm impacts from the wave farm on coastal morphology and the ensuing ocean climate vary spatially. While wave farms mitigate erosion in most parts of the domain, adverse effects or no effects are also seen in some locations. For instance, WECs have the potential to preserve the integrity of dunes in the western region of the island, where erosion is higher in the baseline scenario, but there are some locations where the wave farm does not make any impact, denoted by white in Figure 7c which indicates the same Hs for both scenarios. Additionally, it is observed that the presence of the wave farm does not change the regimes on the eastern side of the island, where the collision regime is prevalent. This is in contrast to the western side of the island, which has lower elevations and does experience overwash and inundation during peak water levels. Bathymetry is a major controller in the spatial variation of the impacts of WECs, since the wave breaking depth is limited [24,40,66]. Bathymetry also impacts the bottom friction, the impact of which effectively changes with depth. Plots of Hs (Figures 7 and 12) show how the variation in wave heights follows the shallow shoals. Wave direction is also likely to play an important role in the spatial variation of WEC impacts on coastal morphology. This is one of the reasons that the relative maximum Hs during Ivan and Katrina (Figures 7c and 12c, respectively) vary spatially.

For both the baseline and wave farm scenarios, the bed elevations are unchanged from the initial (prestorm) profile in both the seaward and landward ends of the transects. This indicates that the storm does not impact the profile in deep water (i.e., greater than ~6 m below sea level). However, it does impact the dunes as well as the subaerial beach and surf zone, i.e., regions of shallow water, and this is also where we see the impacts of WECs. Results show that in the baseline scenario, the sediment is transported 5 to 50 m further inland than in the wave farm scenario for all three transects under both storm conditions. This indicates that wave farms can reduce the magnitude of the physical forces involved in sediment transport (e.g., wave action) and can shorten the distance over which sediment is transported.

Wave farms predominantly mitigate erosion in the western portion of the island. Although this area is uninhabited by humans, it is an important area for wildlife, and is especially critical for the bird habitat and sea turtle nests [67]. It also plays an essential role in protecting mainland Alabama by providing a first line of defense during storm events. Therefore, efforts to protect this portion of the island from coastal erosion and breaching are valuable. Furthermore, the spatial variability seen with this methodology demonstrates the capacity for analyses of this sort to inform ideal configurations of wave farms for optimal mitigation.

The comparison of the results of Ivan and Katrina simulations shows that the wave farms are less effective in changing the Sallenger storm impact scale regime and protecting the integrity of dune structures during intense storms. Because of the low dune elevations on Dauphin Island, erosion and overwash events are observed even during weak storms such as Hurricane Nate, which was a tropical depression when it made landfall in Alabama in 2017 [68]. While a wave farm may not be an effective erosion mitigation strategy for intense storms such as Hurricane Katrina, it can reduce erosion and overwash during weaker storm events and reduce the need for subsequent beach nourishment projects. Impacts of WECs on coastal morphology are more pronounced for Hurricane Ivan simulations

compared to Katrina, meaning storm intensity plays a dynamic role in how effective the WECs are in reducing coastal erosion.

Hydrodynamic changes due to WECs impact the coastal morphodynamics, as expected; however, this study also shows instances where the opposite is true. Local bathymetry and island configuration influence how WECs modify the wave climate in their lee. In fact, impacts of WECs are reversed in sheltered areas and at the locations of breaches. This suggests that consideration of bathymetry and erosion patterns is essential for accurate analysis when analyzing hydrodynamic impacts of WECs in the lee of wave farms. Earlier studies on this topic often lack this consideration.

The amount of sand volume protected from inundation and loss by the wave farm in this case study is comparable to the amount of sand added to beaches during nourishment projects. For example, 250,000 m^3 of sand was added to Dauphin Island for nourishment in 2016 at the cost of USD 7 million [64], and here we show that WECs could have protected 110,000 m^3–210,000 m^3 of sand volume from inundation during Ivan and Katrina, respectively. Considering that beach nourishment is a temporary solution that needs to be repeated each decade, wave farms can be a long-term, cost-effective, and adaptable alternative to current coastal protection methods. The initial cost of wave farms can be high; however, they not only protect the coasts against erosion, they also provide renewable energy to local coastal communities. This can be particularly valuable in the immediate aftermath of a hurricane, when power outages are frequently pervasive. WEC developers aim to increase WEC resiliency so that these devices are able to absorb excessive energy from large storms and rough seas [69]. Studies show that the payback time of WECs associated with the value of the renewable energy they provide is as short as one year [70].

Here, we have explored only the lower limits of the potential for wave energy conversion to mitigate coastal erosion, as we have not accounted for the physical wave-to-WEC or WEC-to-WEC interactions. We have also focused on short-term impacts, and expect that even greater potential for protection may be found with longer-term analyses, particularly with consideration of the changing climate. This work and subsequent studies can be used to explore multicomponent coastal protection strategies combining wave farms, nature-based solutions, and living shorelines, such as coral reefs and salt marshes, to increase coastal adaptability to climate change. Additionally, while we have shown that wave farms can reduce the impacts of coastal processes that are generally favorable to coastal erosion, it is known that overwash and sand deposition on the back barrier during storms are necessary for rollover to occur and to maintain island resilience over time [71,72]. This showcases an interesting trade-off between protection of existing environments and infrastructure versus future island resilience, which may be evaluated in future studies.

5. Conclusions

This study explores the potential for wave energy conversion, conventionally used to generate renewable energy, to simultaneously mitigate coastal erosion. XBeach simulations of baseline (no WECs present) and wave farm scenarios (WECs represented as reduced Hs) under tropical storm conditions on Dauphin Island, AL, demonstrate that wave farms can alleviate the factors that cause coastal erosion, such as wave attack, bed shear stress, and overwash and inundation. We also observe that the consideration of erosion patterns, which has generally been overlooked in related studies, is essential for an accurate analysis when investigating the hydrodynamic impacts of WECs in the lee of wave farms.

Simulations for both Hurricanes Katrina and Ivan yield similar results, supporting the idea that wave farms can be effective in mitigating erosion. A comparison of the results of the storm simulations shows that wave farms are less effective in changing the regime and protecting the integrity of dunes during intense, stronger storms. Thus, the installation of wave farms is a promising approach to mitigating coastal erosion; however, its capacity to alter intense morphodynamic activity is limited. Coastal erosion caused by the strongest hurricanes may be assuaged by more resilient and efficient WEC technologies. Moreover,

the varying impact of the wave farm across the domain emphasizes the need for a thorough analysis when implementing WECs for coastal protection of specific locations.

This work provides a fundamental first step in the use of numerical simulation for assessing the impact of wave energy conversion on coastal hydrodynamics, morphodynamics, and the interactions of both processes. In future work, more detailed numerical wave modeling might be implemented to represent physical wave-to-WEC or WEC-to-WEC interactions and capture the effects of wave dampening and wave reflection functions of WECs on reducing coastal erosion. Since the hydrodynamic impacts may vary based on the WEC type and the wave farm configuration, numerical modeling might be implemented to represent specific WEC types. Longer-term assessments of WECs on coastal morphology might also be conducted to demonstrate even greater potential for coastal resilience, and this study serves as a foundational step forward.

Author Contributions: Conceptualization, C.O. and T.M.; methodology, T.M.; software, D.L.P.; validation, D.L.P.; formal analysis, C.O., T.M. and D.L.P.; investigation, C.O., T.M. and D.L.P.; resources, T.M. and D.L.P.; data curation, C.O. and D.L.P.; writing—original draft preparation, C.O.; writing—review and editing, C.O., T.M. and D.L.P.; visualization, C.O. and D.L.P.; supervision, T.M.; project administration, T.M.; funding acquisition, T.M. All authors have read and agreed to the published version of the manuscript.

Funding: Research reported in this publication was partially supported by an Early-Career Research Fellowship from the Gulf Research Program of the National Academies of Sciences, Engineering, and Medicine. The content is solely the responsibility of the authors and does not necessarily represent the official views of the Gulf Research Program of the National Academies of Sciences, Engineering, and Medicine.

Institutional Review Board Statement: Not applicable.

Informed Consent Statement: Not applicable.

Data Availability Statement: The data presented in this study are available on request from the corresponding author.

Acknowledgments: Research reported in this publication was partially supported by an Early Career Research Fellowship from the Gulf Research Program of the National Academies of Sciences, Engineering, and Medicine. The content is solely the responsibility of the authors and does not necessarily represent the official views of the Gulf Research Program of the National Academies of Sciences, Engineering, and Medicine. Any use of trade, firm, or product names is for descriptive purposes only and does not imply endorsement by the U.S. Government.

Conflicts of Interest: The authors declare no conflict of interest.

References

1. Ozkan, C.; Mayo, T. The Renewable Wave Energy Resource in Coastal Regions of the Florida Peninsula. *Renew. Energy* **2019**, *139*, 530–537. [CrossRef]
2. Dalton, G.J.; Alcorn, R.; Lewis, T. Case study feasibility analysis of the Pelamis wave energy convertor in Ireland, Portugal and North America. *Renew. Energy* **2009**, *35*, 443–455. [CrossRef]
3. Rusu, E.; Onea, F. A review of the technologies for wave energy extraction. *Clean Energy* **2018**, *2*, 10–19. [CrossRef]
4. Luijendijk, A.; Hagenaars, G.; Ranasinghe, R.; Baart, F.; Donchyts, G.; Aarninkhof, S. The State of the World's Beaches. *Sci. Rep.* **2018**, *8*, 6641. [CrossRef]
5. Florida Department of Environmental Protection, Critically Eroded Beaches in Florida. 2019. Available online: https://floridadep.gov/sites/default/files/FDEP-Critically-Eroded-Beaches-2019.pdf (accessed on 7 May 2020).
6. National Ocean Service, Who Moved the Beach? NOAA. 2020. Available online: https://oceanservice.noaa.gov/education/lessons/who_moved_the_beach.html (accessed on 25 May 2020).
7. Masselink, G.; Russell, P.; Rennie, A.; Brooks, S.; Spencer, T. Impacts of climate change on coastal geomorphology and coastal erosion relevant to the coastal and marine environment around the UK. *MCCIP Sci. Rev.* **2020**, 158–189. [CrossRef]
8. NOAA, Economics and Demographics. 2016. Available online: https://coast.noaa.gov/states/fast-facts/economics-and-demographics.html (accessed on 6 April 2020).
9. NOAA, National Coastal Population Report. 2013. Available online: http://stateofthecoast.noaa.gov (accessed on 6 April 2020).

10. Camelo, J.; Mayo, T.; Gutmann, E.D. Projected Climate Change Impacts on Hurricane Storm Surge Inundation in the Coastal United States. *Front. Built Environ.* **2020**, *6*, 207. [CrossRef]
11. Taherkhani, M.; Vitousek, S.; Barnard, L.; Frazer, N.; Anderson, T.R.; Fletcher, C.H. Sea-level rise exponentially increases coastal flood frequency. *Sci. Rep.* **2020**, *10*, 6466. [CrossRef]
12. Morris, R.L.; Boxshall, A.; Swearer, S.E. Climate-resilient coasts require diverse defence solutions. *Nat. Clim. Chang.* **2020**, *10*, 485–487. [CrossRef]
13. Temmerman, S.; Meire, P.; Bouma, T.J.; Herman, P.M.J.; Ysebaert, T.; De Vriend, H.J. Ecosystem-based coastal defence in the face of global change. *Nature* **2013**, *504*, 79–83. [CrossRef] [PubMed]
14. Kibler, K.M.; Kitsikoudis, V.; Donnelly, M.; Spiering, D.W.; Walters, L. Flow–Vegetation Interaction in a Living Shoreline Restoration and Potential Effect to Mangrove Recruitment. *Sustainability* **2019**, *11*, 3215. [CrossRef]
15. Seddon, N.; Daniels, E.; Davis, R.; Chausson, A.; Harris, R.; Hou-Jones, X.; Huq, S.; Kapos, V.; Mace, G.M.; Rizvi, A.R.; et al. Global recognition of the importance of nature-based solutions to climate change impacts. *Glob. Sustain.* **2020**, *3*, e15. [CrossRef]
16. ASBPA, National Beach Nourishment Database. 2019. Available online: https://gim2.aptim.com/ASBPANationwideRenourishment/ (accessed on 8 April 2020).
17. US Department of the Interior. Salazar, Menendez Announce $29 Million to Restore Ellis Island Seawall, Historic Structures under President's Recovery Plan. 2016. Available online: https://www.doi.gov/news/pressreleases/Salazar-Menendez-Announce-29-Million-to-Restore-Ellis-Island-Seawall-Historic-Structures-under-Presidents-Recovery-Plan (accessed on 8 April 2020).
18. Copping, A.; Sather, N.; Hanna, L.; Whiting, J.; Zydlewski, G.; Staines, G.; Gill, A.; Hutchison, A.; O'Hagan, A.; Simas, T.; et al. Annex IV 2016 State of the Science Report: Environmental Effects of Marine Renewable Energy Development around the World. 2016. Available online: https://tethys.pnnl.gov/sites/default/files (accessed on 5 January 2022).
19. Lancaster, O.; Cossu, R.; Baldock, T.E. Experimental investigation into 3D scour processes around a gravity based Oscillating Water Column Wave Energy Converter. *Coast. Eng.* **2020**, *161*, 103754. [CrossRef]
20. Bergillos, R.J.; López-Ruiz, A.; Medina-López, E.; Moñino, A.; Ortega-Sánchez, M. The role of wave energy converter farms on coastal protection in eroding deltas, Guadalfeo, southern Spain. *J. Clean. Prod.* **2018**, *171*, 356–367. [CrossRef]
21. Rodriguez-Delgado, C.; Bergillos, R.J.; Ortega-Sánchez, M.; Iglesias, G. Protection of gravel-dominated coasts through wave farms: Layout and shoreline evolution. *Sci. Total Environ.* **2018**, *636*, 1541–1552. [CrossRef]
22. Rodriguez-Delgado, C.; Bergillos, R.J.; Ortega-Sánchez, M.; Iglesias, G. Wave farm effects on the coast: The alongshore position. *Sci. Total Environ.* **2018**, *640–641*, 1176–1186. [CrossRef]
23. Abanades, J.; Flor-Blanco, G.; Flor, G.; Iglesias, G. Dual wave farms for energy production and coastal protection. *Ocean Coast. Manag.* **2018**, *160*, 18–29. [CrossRef]
24. Abanades, J.; Greaves, D.; Iglesias, G. Coastal defence through wave farms. *Coast. Eng.* **2014**, *91*, 299–307. [CrossRef]
25. Rijnsdorp, D.P.; Hansen, J.E.; Lowe, R.J. Understanding coastal impacts by nearshore wave farms using a phase-resolving wave model. *Renew. Energy* **2020**, *150*, 637–648. [CrossRef]
26. Rodriguez-Delgado, C.; Bergillos, R.J.; Iglesias, G. Dual wave farms for energy production and coastal protection under sea level rise. *J. Clean. Prod.* **2019**, *222*, 364–372. [CrossRef]
27. Stokes, C. *Coastal Impacts in the Lee of a Wave Energy Site: Waves, Beach Morphology and Water-Users*; Wave Hub; University of Plymouth: Cornwall, UK, 2015.
28. Stokes, C.; Conley, D. Modelling Offshore Wave farms for Coastal Process Impact Assessment: Waves, Beach Morphology, and Water Users. *Energies* **2018**, *11*, 2517. [CrossRef]
29. Xu, C.; Huang, Z. A dual-functional wave-power plant for wave-energy extraction and shore protection: A wave-flume study. *Appl. Energy* **2018**, *229*, 963–976. [CrossRef]
30. Rodriguez-Delgado, C.; Bergillos, R.J.; Iglesias, G. Dual wave farms and coastline dynamics: The role of inter-device spacing. *Sci. Total Environ.* **2019**, *646*, 1241–1252. [CrossRef]
31. Abanades, J.; Greaves, D.; Iglesias, G. Coastal defence using wave farms: The role of farm-to-coast distance. *Renew. Energy* **2015**, *75*, 572–582. [CrossRef]
32. Abanades, J.; Greaves, D.; Iglesias, G. Wave farm impact on the beach profile: A case study. *Coast. Eng.* **2014**, *86*, 36–44. [CrossRef]
33. Abanades, J.; Greaves, D.; Iglesias, G. Wave farm impact on beach modal state. *Mar. Geol.* **2015**, *361*, 126–135. [CrossRef]
34. Bergillos, R.J.; Rodriguez-Delgado, C.; Allen, J.; Iglesias, G. Wave energy converter configuration in dual wave farms. *Ocean Eng.* **2019**, *178*, 204–214. [CrossRef]
35. Bergillos, R.J.; Rodriguez-Delgado, C.; Allen, J.; Iglesias, G. Wave energy converter geometry for coastal flooding mitigation. *Sci. Total Environ.* **2019**, *668*, 1232–1241. [CrossRef] [PubMed]
36. Bergillos, R.J.; Rodriguez-Delgado, C.; Iglesias, G. Wave farm impacts on coastal flooding under sea-level rise: A case study in southern Spain. *Sci. Total Environ.* **2019**, *653*, 1522–1531. [CrossRef] [PubMed]
37. Bergillos, R.J.; Rodriguez-Delgado, C.; Iglesias, G. *Ocean Energy and Coastal Protection-A Novel Strategy for Coastal Management Under Climate Change*; Springer Briefs in Energy: Cham, Switzerland, 2020.
38. Ozkan, C.; Perez, K.; Mayo, T. The impacts of wave energy conversion on coastal morphodynamics. *Sci. Total Environ.* **2020**, *712*, 136424. [CrossRef]
39. Gonzalez-Santamaria, R.; Zou, Q.P.; Pan, S. Impacts of a Wave Farm on Waves, Currents and Coastal Morphology in South West England. *Estuaries Coasts* **2013**, *38*, 159–172. [CrossRef]

40. Jones, C.; Chang, G.; Raghukumar, K.; McWilliams, S.; Dallman, A.; Roberts, J. Spatial Environmental Assessment Tool (SEAT): A Modeling Tool to Evaluate Potential Environmental Risks Associated with Wave Energy Converter Deployments. *Energies* **2018**, *11*, 2036. [CrossRef]
41. USGS, The National Map-Advanced Viewer. 2017. Available online: https://viewer.nationalmap.gov/advanced-viewer/ (accessed on 7 May 2020).
42. NREL, RE Atlas. 2020. Available online: https://maps.nrel.gov/re-atlas/?aL=0&bL=groad&cE=0&lR=0&mC=40.21244%2C-91.625976&zL=4 (accessed on 30 April 2020).
43. Morton, R.A.; Miller, T.L.; Moore, L.J. *National Assessment of Shoreline Change: Part 1 Historical Shoreline Changes and Associated Coastal Land Loss along the U.S. Gulf of Mexico*; USGS: St. Petersburg, FL, USA, 2004. Available online: https://pubs.usgs.gov/of/2004/1043/ofr-2004-1043.pdf (accessed on 30 April 2020).
44. Givens, J. Dauphin Island's Shifting Sands, Mob. Bay Mag. 2019. Available online: https://mobilebaymag.com/dauphin-islands-shifting-sands (accessed on 16 May 2020).
45. Sallenger, A. Storm impact scale for barrier islands. *J. Coast. Res.* **2000**, *16*, 890–895.
46. Cebrian, J. Living Shoreline: Using Natural and Artificial Breakwaters in Shoreline Restoration and Conservation | Dauphin Island Sea Lab. 2019. Available online: https://www.disl.org/about/faculty/faculty-projects/living-shoreline-using-natural-and-artificial-breakwaters-in-shoreline-rest (accessed on 8 May 2020).
47. Hansen, M.; Sallenger, A.H. Barrier Island Vulnerability to Breaching: A Case Study on Dauphin Island, Alabama. In Proceedings of the Coastal Sediments '07—Proceedings of 6th International Symposium on Coastal Engineering and Science of Coastal Sediment Processes, New Orleans, LA, USA, 13–17 May 2007; pp. 2002–2010. [CrossRef]
48. National Hurricane Center-NOAA. *Costliest U.S. Tropical Cyclones Tables Updated*; National Hurricane Center-NOAA: Miami, FL, USA, 2018. Available online: https://www.nhc.noaa.gov/news/UpdatedCostliest.pdf (accessed on 30 April 2020).
49. FEMA. Hurricane Ivan Overview. 2016. Available online: https://www.fema.gov/hurricane-ivan-overview (accessed on 30 April 2020).
50. Gaul, G.M. On the Alabama Coast, the Unluckiest Island in America, Yale E360. 2019. Available online: https://e360.yale.edu/features/on-the-alabama-coast-the-unluckiest-island-in-america (accessed on 19 May 2020).
51. Knabb, R.D.; Rhome, J.R.; Brown, D.P. Tropical Cyclone Report Hurricane Katrina 23–30 August 2005. 2005. Available online: https://www.nhc.noaa.gov/data/tcr/AL122005_Katrina.pdf (accessed on 30 April 2020).
52. Roelvink, D.; Reniers, A.; van Dongeren, A.; van Thiel de Vries, J.; McCall, R.; Lescinski, J. Modelling storm impacts on beaches, dunes and barrier islands. *Coast. Eng.* **2009**, *56*, 1133–1152. [CrossRef]
53. Roelvink, D.; Van Dongeren, A.; McCall, R.; Hoonhout, B.; Van Rooijen, A.; Van Geer, P.; De Vet, L.; Nederhoff, K. XBeach Documentation: Release XBeach v1.23.5527 XBeachX Final. 2018. Available online: https://oss.deltares.nl/documents/48999/2022076/Documentation_XBeach-v1.23.5527-XBeachX_FINAL.pdf/d366edea-db7c-1c2e-4295-a7222c8970bc?version=1.0 (accessed on 11 May 2020).
54. Passeri, D.L.; Bilskie, M.V.; Plant, N.G.; Long, J.W.; Hagen, S.C. Dynamic modeling of barrier island response to hurricane storm surge under future sea level rise. *Clim. Chang.* **2018**, *149*, 413–425. [CrossRef]
55. Enríquez, A.R.; Marcos, M.; Falqués, A.; Roelvink, D. Assessing beach and dune erosion and vulnerability under sea level rise: A Case study in the Mediterranean Sea. *Front. Mar. Sci.* **2019**, *6*, 4. [CrossRef]
56. Passeri, D.L.; Long, J.W.; Plant, N.G.; Bilskie, M.V.; Hagen, S.C. The influence of bed friction variability due to land cover on storm-driven barrier island morphodynamics. *Coast. Eng.* **2018**, *132*, 82–94. [CrossRef]
57. Danielson, J.J.; Brock, J.C.; Howard, D.M.; Gesch, D.B.; Bonisteel-Cormier, J.M.; Travers, L.J. *Topobathymetric Model of Mobile Bay, Alabama*; Data Series 769; U.S. Geological Survey: St. Petersburg, FL, USA, 2013. Available online: https://pubs.usgs.gov/ds/769/ (accessed on 27 May 2020).
58. Ergin, A. *Coastal Engineering*; Metu Press: Ankara, Turkey, 2009.
59. Fernandez, H.; Iglesias, G.; Carballo, R.; Castro, A.; Fraguela, J.A.; Taveira-Pinto, F.; Sanchez, M. The new wave energy converter WaveCat: Concept and laboratory tests. *Mar. Struct.* **2012**, *29*, 58–70. [CrossRef]
60. Bilskie, M.V.; Hagen, S.C.; Medeiros, S.C.; Cox, A.T.; Salisbury, M.; Coggin, D. Data and numerical analysis of astronomic tides, wind-waves, and hurricane storm surge along the northern Gulf of Mexico. *J. Geophys. Res. Ocean.* **2016**, *121*, 3625–3658. [CrossRef]
61. Luettich, R.A.; Westerink, J.J.; Scheffner, N.W. *ADCIRC: An Advanced Three-Dimensional Circulation Model for Shelves Coasts and Estuaries, Report 1: Theory and Methodology of ADCIRC-2DDI and ADCIRC-3DL*; US Army Corps of Engineers: Washington, DC, USA, 1992.
62. Vethamony, P.; Aboobacker, V.M.; Menon, H.B.; Kumar, K.A.; Cavaleri, L. Superimposition of wind seas on pre-existing swells off Goa coast. *J. Mar. Syst.* **2011**, *87*, 47–54. [CrossRef]
63. Badulin, S.I.; Korotkevich, A.O.; Resio, D.; Zakharov, V.E. Wave-wave interactions in wind-driven mixed seas. In Proceedings of the Rogue Waves 2008 Workshop, Brest, France, 13–15 October 2008; pp. 77–86.
64. Buhring, B. Dauphin Island East End Beach and Barrier Island Restoration Project. 2017. Available online: https://sportdocbox.com/Surfing_and_Body_Boarding/71550785-Dauphin-island-east-end-beach-and-barrier-island-restoration-project-beau-buhring-south-coast-engineers.html (accessed on 18 March 2020).

65. Wang, Y.; Yu, Q.; Gao, S. Relationship between bed shear stress and suspended sediment concentration: Annular flume experiments. *Int. J. Sediment Res.* **2011**, *26*, 513–523. [CrossRef]
66. O'Dea, A.; Haller, M.C.; Özkan-Haller, H.T. The impact of wave energy converter arrays on wave-induced forcing in the surf zone. *Ocean Eng.* **2018**, *161*, 322–336. [CrossRef]
67. Ingram, D.K.; Isaacs, J.M.; Gleason, J.S.; Reynolds, M.O.; Reetz, K.K.; Yadamec, T.J. Loggerhead Nesting Ecology in Baldwin and Mobile Counties, Alabama, USA, 2003–2012, Spanish Fort. 2014. Available online: https://www.researchgate.net/publication/261617294 (accessed on 16 September 2020).
68. Coogan, J.; Webb, B.; Smallegan, S.; Puleo, J. Geomorphic changes measured on Dauphin Island, AL, during Hurricane Nate. *Shore Beach* **2019**, *87*, 16–22. [CrossRef]
69. NREL. How Wave Energy Could Go Big by Getting Smaller. 2021. Available online: https://www.nrel.gov/news/program/2021/how-wave-energy-could-go-big-by-getting-smaller.html (accessed on 31 December 2021).
70. Thomson, R.C.; Harrison, G.P.; Chick, J.P. Full life cycle assessment of a wave energy converter. In Proceedings of the IET Conference on Renewable Power Generation (RPG 2011), Edinburgh, UK, 6–8 September 2011; pp. 1–6.
71. Masselink, G.; Hughes, M.G. *Introduction to Coastal Processes and Geomorphology*, 2nd ed.; Routledge: London, UK, 2014.
72. Lorenzo-Trueba, J.; Ashton, A.D. Rollover, drowning, and discontinuous retreat: Distinct modes of barrier response to sea-level rise arising from a simple morphodynamic model. *J. Geophys. Res. Earth Surf.* **2014**, *119*, 779–801. [CrossRef]